

AD-A202 594



DTIC
ELECTE
JAN 18 1989
S CH D

HYBRID CALCULATION OF INVARIANT MOMENTS

THESIS

Vicky Lynn Robinson
Captain, USAF

AFIT/GEO/ENG/88D-3

DEPARTMENT OF THE AIR FORCE
AIR UNIVERSITY

AIR FORCE INSTITUTE OF TECHNOLOGY

Wright-Patterson Air Force Base, Ohio

DISTRIBUTION STATEMENT A

Approved for public release;
Distribution Unlimited

89

1 17 157

AFIT/GEO/ENG/88D-3

HYBRID CALCULATION OF INVARIANT MOMENTS

THESIS

Vicky Lynn Robinson
Captain, USAF

AFIT/GEO/ENG/88D-3



Approved for public release; distribution unlimited

AFIT/GEO/ENG/88D-3

HYBRID CALCULATION OF INVARIANT MOMENTS

THESIS

Presented to the Faculty of the School of Engineering
of the Air Force Institute of Technology
Air University
In Partial Fulfillment of the
Requirements for the Degree of
Master of Science in Electrical Engineering

Vicky Lynn Robinson, B.S.
Captain, USAF

December, 1988

Approved for public release; distribution unlimited

Preface

This thesis demonstrated the feasibility of using optically generated moments for pattern recognition. Detour phase holograms were used to produce the appropriate wavefronts and digital postprocessing was performed to obtain a position, scale, rotation invariant feature set.

Many people contributed to this research. First, and foremost, I would like to thank my mom and dad for their unending love and support. I would also like to thank the members of Diakonos at Christian Life Center, especially Judy Chaboty, Suzy Racicot, and Phyllis Wampler, for their prayers throughout the past 18 months. I would like to thank my thesis advisor, Dr. Steven Rogers, for his unending encouragement and technical support. I'm also grateful to Capt Tom Walrond, Capt Tim Childress, Capt Dave Haralson, Capt Pete Collins and Rick Patton for their aid in obtaining alot of the optical equipment used in the experiment. I would also like to thank Capt Ken Fielding and Lt Col James Lupo for their help in producing the necessary computer generated holograms. Finally, I appreciated the support and encouragement provided by the rest of the GEO-88D section.

Vicky Lynn Robinson

Accession For	
NTIS GRA&I	<input checked="checked" type="checkbox"/>
DTIC TAB	<input type="checkbox"/>
Unannounced	<input type="checkbox"/>
Justification	
By	
Institution/	
Availability Codes	
Avail and/or	
Dist Special	
A-1	

Table of Contents

	Page
Preface	ii
Table of Contents	iii
List of Figures	v
List of Tables	vii
Abstract	viii
I. Introduction	1
Approach and Scope	1
Organization	2
II. Summary of Current Knowledge	3
Moments	3
Optical Moment Generator	6
Computer Generated Holograms	7
Euclidean Distance	12
III. Procedures	14
Transparency Production	14
Hologram Tests	15
Moment Calculation	18
Data Collection	19

	Page
IV. Data Analysis	24
Moment Values	24
Distance Calculations	24
Results	25
V. Conclusions and Recommendations	34
Conclusions	34
Recommendations	34
Appendix A. Hologram Production	37
Program	37
Variables	38
Appendix B. Photoreduction Process	42
Appendix C. CGH Plots	44
Appendix D. Intensity Line Profiles of the $x^p y^q$ Wavefronts	50
Appendix E. Program for Calculating PSRI Moments	58
Bibliography	63
Vita	65

List of Figures

Figure	Page
1. Optical Moment Generator	7
2. Computer Generated Hologram Cell	9
3. Optical Wavefront Generator	10
4. Distance Example	12
5. x CGH: Linear Ramp in Intensity	16
6. Computer Generated Hologram Test Setup	17
7. Resultant Wavefront From "x" CGH - - x Direction	18
8. Resultant Wavefront From "x" CGH - - y Direction	19
9. Alignment Card	20
10. Moment Generation Setup	21
11. Experimental Setup	22
12. Thresholded, Scaled Intensity Pattern	23
13. Effect of Optical System on the Beam	23
14. Distance Calculation Program	26
15. Dekacon Photoreduction System	43
16. x CGH Plot	45
17. x^2 CGH Plot	46
18. xy CGH Plot	47
19. x^2y CGH Plot	48
20. x^3 CGH Plot	49
21. Beginning Beam Wavefront Profiles	51
22. " x " Wavefront Profiles	52
23. x^2 Wavefront Profiles	53
24. xy Wavefront Profiles	54

Figure		Page
25.	x^2y Wavefront Profiles	55
26.	x^3 Wavefront Profiles	56
27.	End Beam Wavefront Profiles	57

List of Tables

Table		Page
1.	Experimental Data	28
2.	Ordinary Moments	30
3.	PSRI Moments	31
4.	Ordinary Moment Distances	32
5.	PSRI Moment Distances	33

Abstract

This thesis investigated a hybrid system for computing a position, scale, rotation invariant (PSRI) feature set. Specifically, the low order ordinary moments of a set of objects were optically calculated. This process required the production of computer generated holograms with amplitude transmittance. The detour phase hologram, a binary method, was used to produce the appropriate wavefronts of the form $x^p y^q$. Each wavefront was imaged onto the object plane. The Fourier transform of the product of these two transmittances was taken and the resultant intensity pattern recorded. The center intensity value was found by using a frame grabber and the Image-Pro software. The result was the ordinary moment of the object. The moment values were digitally processed to form a PSRI feature set. The moments, both ordinary and PSRI, were tested for pattern recognition possibilities. The Euclidean distances between the objects were calculated, revealing the separation necessary for pattern recognition. (A) ←

HYBRID CALCULATION OF INVARIANT MOMENTS

I. Introduction

The Air Force is actively investigating pattern recognition machines which can be incorporated into autonomous weapons. Feature extraction is an essential part of the pattern recognition process. An applicable feature set is any set of information which can be used to identify the objects of interest. One such feature set is the moments of the object. This feature set has not been extensively used due to excessive digital processing time. This thesis will research the feasibility of the optical generation of ordinary moments with digital postprocessing to produce invariance, otherwise known as the hybrid calculation of invariant moments. In addition, the ability of these moments to identify several objects will be investigated.

Approach and Scope

The first task in this thesis is to research the current knowledge of the moment feature set and its use in pattern recognition. The second step is to produce the computer generated holograms needed for the optical computation of moments. The first four moment orders (zeroth, first, second, and third) will be calculated. This requires holograms which create wavefronts that vary according to the following functions: x , x^2 , xy , x^2y , and x^3 . Third, the holograms are tested for accuracy and the moments of six objects are optically calculated. It is assumed that the objects have been segmented before the recognition process is begun. This research will attempt to distinguish the following objects: square, circle, triangle, truck, tank, and airplane. Fourth, digital postprocessing will be used to produce a position, scale, rotation invariant (PSRI) feature set. Finally, both the ordinary and PSRI feature

sets will be tested for pattern recognition possibilities, i.e., the Euclidean distances between the moments of the objects will be calculated.

Organization

This thesis begins with a summary of the current knowledge of the moment feature set. It briefly discusses moments and details an optical system for their calculation. An integral part of this system is the computer generated holograms used to obtain the appropriate wavefronts. The method used to generate these holograms is detailed. The experiments performed to test the system are described in Chapter III. The results are discussed in Chapter IV, and concluding remarks are contained in Chapter V.

II. Summary of Current Knowledge

The use of moments for pattern recognition was introduced by Ming-Kuei Hu in 1962 (11; 17:920). However, due to the large computational load, this feature set has not been extensively used. It currently takes 1.16×10^8 operations per second to compute eleven moments of a 512×512 pixel image in 30 msec (6:395). Also, large amounts of memory are required to convert the analog form to a digital image. Therefore, real-time digital processing is very difficult (6:395). An optical implementation of this system would alleviate these problems and make moments a very desirable and applicable feature set for pattern recognition work (15).

This chapter details the previous work which has been done with moments. Moments are first defined. An explanation is then given as to how they can be used for pattern recognition. This includes the mathematics for producing a position, scale, rotation invariant (PSRI) feature set. Next, an optical setup for calculating moments is described. Section III details the production of the computer generated holograms (CGHs) needed for the optical computations. The final section explains Euclidean distance and its use in pattern recognition.

Moments

The $(p + q)^{th}$ ordinary moment of an object is defined as

$$m_{pq} = \int_{-\infty}^{\infty} \int_{-\infty}^{\infty} x^p y^q f(x, y) dx dy \quad (1)$$

Teague has shown that moments can be used to reconstruct letters. Combining up through the 15th order moments results in a letter which appears to replicate the original (17:923-924). This indicates that the moment feature set is applicable for pattern recognition.

The moments contain information necessary to classify the object. For example (3:442; 15),

1. m_{00} provides an estimate of the scale of the object,
2. m_{01} and m_{10} provide an indication of the object's location, and
3. m_{20}/m_{02} provides the height-to-width ratio of the object.

Thus, ordinary moments are highly variable to changes in position, scale, and rotation of the object. However, these sensitivities can be eliminated. First, central moments, μ_{pq} , can be defined with respect to the centroid of the object, making them insensitive to object shifts. They can be related to the ordinary moments as follows (17:925):

$$\mu_{pq} = \sum_{r=0}^p \sum_{s=0}^q \binom{p}{r} \binom{q}{s} (-\bar{x})^{p-r} (-\bar{y})^{q-s} m_{rs} \quad (2)$$

where

$$\bar{x} \equiv \frac{m_{10}}{m_{00}}, \quad \bar{y} \equiv \frac{m_{01}}{m_{00}} \quad (3)$$

and the combination of "a" things taken "b" at a time is defined as:

$$\binom{a}{b} \equiv \frac{a!}{b!(a-b)!} \quad (4)$$

Scale variations can be eliminated by assuming that the scaling is due to a change in the range of the object. In this case, the new object is defined as

$$f'(x, y) = f\left(\frac{x}{\lambda}, \frac{y}{\lambda}\right) \quad (5)$$

where λ is the ratio of the two ranges, $\lambda = R/R'$. The moments become

$$m'_{pq} = \int_{-\infty}^{\infty} \int_{-\infty}^{\infty} x^p y^q f\left(\frac{x}{\lambda}, \frac{y}{\lambda}\right) dx dy \quad (6)$$

Let $x' = \frac{x}{\lambda}$ and $y' = \frac{y}{\lambda}$ then $x = \lambda x'$, $y = \lambda y'$, $dx = \lambda dx'$, and $dy = \lambda dy'$. Therefore,

$$\begin{aligned} m'_{pq} &= \int_{-\infty}^{\infty} \int_{-\infty}^{\infty} (\lambda x')^p (\lambda y')^q f(x', y') \lambda^2 dx' dy' \\ &= \lambda^{(2+p+q)} \int_{-\infty}^{\infty} \int_{-\infty}^{\infty} x'^p y'^q f(x', y') dx' dy' \\ &= \lambda^{(2+p+q)} m_{pq} \end{aligned} \quad (7)$$

From equation 7,

$$m'_{00} = \lambda^2 m_{00}, \quad m'_{10} = \lambda^3 m_{10}, \quad \text{and} \quad m'_{01} = \lambda^3 m_{01}.$$

Therefore,

$$\bar{x}' = \lambda \bar{x} \quad \text{and} \quad \bar{y}' = \lambda \bar{y}.$$

The scaled central moments become

$$\begin{aligned} \mu'_{pq} &= \sum_{r=0}^p \sum_{s=0}^q \binom{p}{r} \binom{q}{s} (-\lambda \bar{x})^{p-r} (-\lambda \bar{y})^{q-s} \lambda^{(2+r+s)} m_{rs} \\ &= \sum_{r=0}^p \sum_{s=0}^q \binom{p}{r} \binom{q}{s} (-\bar{x})^{p-r} (-\bar{y})^{q-s} \lambda^{(2+r+s)+(p-r)+(q-s)} m_{rs} \\ &= \lambda^{(p+q+2)} \mu_{pq} \end{aligned} \tag{8}$$

Define (17:925):

$$\eta_{pq} = \frac{\mu_{pq}}{\mu_{00}^{(2+p+q)/2}} \tag{9}$$

Then, from equations 8 and 9, η_{pq} of a scaled object is:

$$\begin{aligned} \eta'_{pq} &= \frac{\mu'_{pq}}{\mu_{00}^{(2+p+q)/2}} \\ &= \frac{\lambda^{2+p+q} \mu_{pq}}{(\mu_{00} \lambda^2)^{(2+p+q)/2}} \\ &= \frac{\lambda^{2+p+q} \mu_{pq}}{\lambda^{2+p+q} \mu_{00}^{(2+p+q)/2}} \\ &= \eta_{pq} \end{aligned}$$

Therefore, η_{pq} , as defined in equation 9, is invariant to scaling of the object.

From the theory of invariant moments, combining these moments as shown below produces a rotation invariance. A PSRI feature set results (6:395).

$$\phi_1 = \eta_{20} + \eta_{02} \tag{10}$$

$$\phi_2 = (\eta_{20} - \eta_{02})^2 + 4\eta_{11}^2 \tag{11}$$

$$\phi_3 = (\eta_{30} - 3\eta_{12})^2 + (3\eta_{21} - \eta_{03})^2 \quad (12)$$

$$\phi_4 = (\eta_{30} + \eta_{12})^2 + (\eta_{21} + \eta_{03})^2 \quad (13)$$

$$\begin{aligned} \phi_5 = & (\eta_{30} - 3\eta_{12})(\eta_{30} + \eta_{12})[(\eta_{30} + \eta_{12})^2 - 3(\eta_{21} + \eta_{03})^2] + \\ & (3\eta_{21} - \eta_{03})(\eta_{21} + \eta_{03})[3(\eta_{30} + \eta_{12})^2 - (\eta_{21} + \eta_{03})^2] \end{aligned} \quad (14)$$

$$\phi_6 = (\eta_{20} - \eta_{02})[(\eta_{30} + \eta_{12})^2 - (\eta_{21} + \eta_{03})^2] + 4\eta_{11}(\eta_{30} + \eta_{12})(\eta_{21} + \eta_{03}) \quad (15)$$

$$\begin{aligned} \phi_7 = & (3\eta_{21} - \eta_{03})(\eta_{30} + \eta_{12})[(\eta_{30} + \eta_{12})^2 - 3(\eta_{21} + \eta_{03})^2] - \\ & (\eta_{30} - 3\eta_{12})(\eta_{21} + \eta_{03})[3(\eta_{30} + \eta_{12})^2 - (\eta_{21} + \eta_{03})^2] \end{aligned} \quad (16)$$

As stated earlier, the main drawback of a pattern recognition system implementing these algorithms is the large amount of processing time needed to compute the ordinary moments. The next section details the use of optical computation to alleviate this problem.

Optical Moment Generator

Several experimenters have implemented optical systems for generating the ordinary moments of objects (2;4;5;6;7;18). The main variation between these systems is the holograms used. This thesis implements the system proposed by David Casasent and Demitri Psaltis (6). The system is shown schematically in Figure 1 (6:395).

The laser light is incident on plane P_1 , whose transmittance is $f(x,y)$. This function is imaged onto plane P_2 , where it is multiplied by the transmittance $g(x,y) = x^p y^q$. The Fourier transform of this product is taken by lens L_3 . The wavefront at plane P_3 is:

$$\mathcal{U}(\omega_x, \omega_y) = \int_{-\infty}^{\infty} \int_{-\infty}^{\infty} f(x,y) x^p y^q e^{-j(\omega_x x + \omega_y y)} dx dy. \quad (17)$$

The on-axis value is

$$\mathcal{U}(0,0) = \int_{-\infty}^{\infty} \int_{-\infty}^{\infty} f(x,y) x^p y^q dx dy. \quad (18)$$

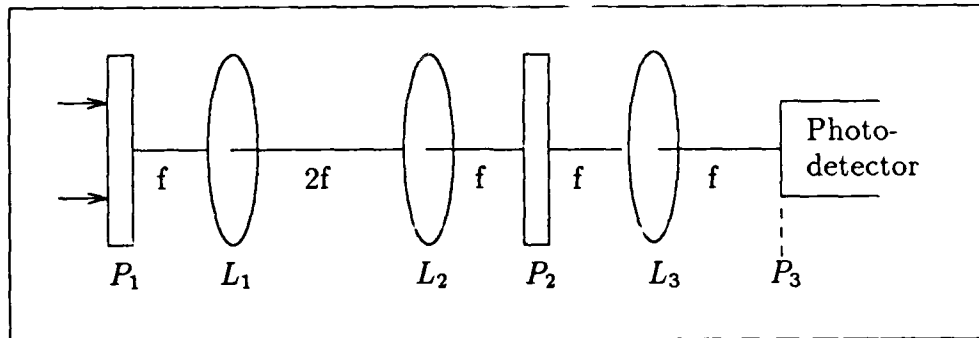


Figure 1. Optical Moment Generator

These, by definition, are the ordinary moments of the object represented by $f(x,y)$ (6:396). A detector is placed on-axis at plane P_3 . The $(p+q)^{th}$ moment is the value of the center of the resultant intensity pattern (1:51). This system requires a different mask for each moment order generated. Once the appropriate moments have been generated, digital postprocessing can be used to obtain a position, scale, rotation invariant moment set, per equations 2 and 9 through 16.

In order to compute the moments, computer generated holograms (CGHs) will be used to create the $x^p y^q$ wavefront. The procedure used to produce these holograms is explained in the following section.

Computer Generated Holograms

Computer generated holograms are "produced as graphical output from a digital computer" (13:121). The computer requires only a mathematical representation of the desired wavefront. This process allows the formulation of wavefronts which could not be generated by conventional optical means (13:121).

Various coding schemes can convert the desired wavefront into a real, non-negative function which can be used to generate the desired outcome through optical means (13:122). The coding scheme used in this thesis is the detour phase method introduced by Brown and Lohmann in 1966 (13:126).

The detour phase method differs from other schemes as follows (13:126-127):

1. the transmission of the hologram is binary,
2. the hologram can record the amplitude and phase of any complex valued function, and
3. the hologram is not recorded with the explicit use of a carrier frequency or a bias, as in the off-axis reference beam holograms.

To fabricate this type of a hologram, the desired wavefront, $A(x, y)e^{j\phi(x, y)}$, is sampled at equally spaced intervals. The spacing must be less than $1/U$, where U is the two-sided spatial bandwidth of the wavefront in the direction of sampling (13:127). Since the wavefront to be produced for this thesis is an amplitude transmittance, $x^p y^q$, there is no phase term, ($\phi(x, y) = 0$). Also, the Fourier transform of $x^p y^q$ is some form of a derivative of a delta, so the spatial bandwidth is essentially zero (9:317). Based on this, the sample spacing must be less than infinity ($1/0$). In reality, there is a spatial limit associated with the finite size of the hologram, but the bandwidth is still very small. Therefore, the sample spacing is not critical to the formation of the wavefront. However, it is important in the separation of the diffracted orders in the Fourier transform (FT) plane. This problem will be addressed in section III.

The paper on which the hologram is to be printed is divided into a number of equally sized cells, with the center to center separation of the cells determined by the sample spacing. The coordinates (n, m) designate the cell located in column n and row m . The phase and amplitude of the wavefront, sampled at the center of each cell, determine the location and size of the rectangle printed inside the cell. The dimensions and placement of the rectangles are determined by the following formulas (13:127, 133):

$$h_{nm} = A_{nm} d_y \quad (19)$$

$$w_{nm} = w \quad (20)$$

$$c_{nm} = d_x(2\pi n + \phi_{nm})/2\pi \quad (21)$$

where d_x and d_y are the sample spacing in the x and y directions, respectively, h_{nm} is the height of the rectangle, w is the width of the rectangle, c_{nm} is the location of the center of the rectangle, ϕ_{nm} is the sampled phase, A_{nm} is the sampled amplitude, and n is an integer (Figure 2). In order to obtain the best tradeoff between intensity

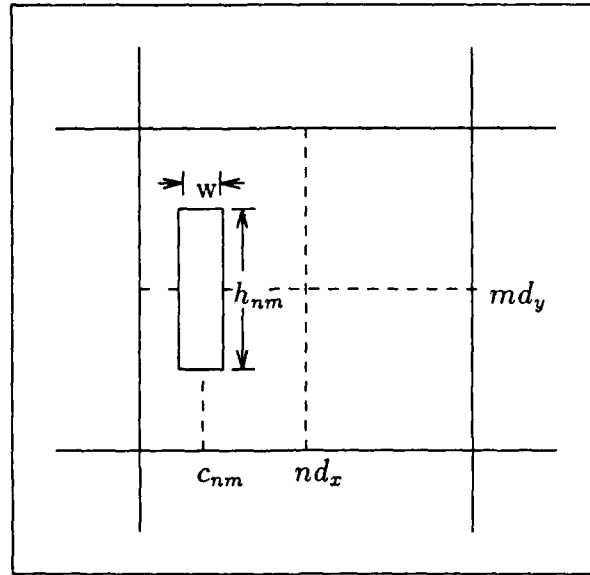


Figure 2. Computer Generated Hologram Cell

and wavefront quality, the width of every rectangle should be one half the width of the cell (16:498-499).

The amplitude is normalized so that the maximum value over the entire wavefront is one. This will result in rectangle heights proportional to the amplitude of the wavefront, and with maxima equal to the height of the cell. The use of equation (21) to determine the center of the rectangle will produce a wave without phase-dependent noise (13:133).

The wavefront to be constructed in this effort has a amplitude transmittance, $x^p y^q$. Setting ϕ_{nm} , in equation (21), to zero yields $c_{nm} = nd_x$. In other words, for an amplitude hologram, the rectangles are all centered in their respective cells.

The program used to generate these holograms is detailed in Appendix A. Once the printout is obtained, it is photoreduced onto a glass plate. This process is detailed in Appendix B.

The hologram described above results in a series of equally spaced rectangles of fixed width and varying height. The transmittance function is (13:128):

$$t(x, y) = \sum_{n=1}^N \sum_{m=1}^M \text{rect}[(x - nd_x)/w] \text{rect}[(y - md_y)/h_{nm}] \quad (22)$$

By placing this hologram in the optical system shown in Figure 3, the desired wavefront is obtained. The wavefront incident on plane P_2 is the FT of the CGH

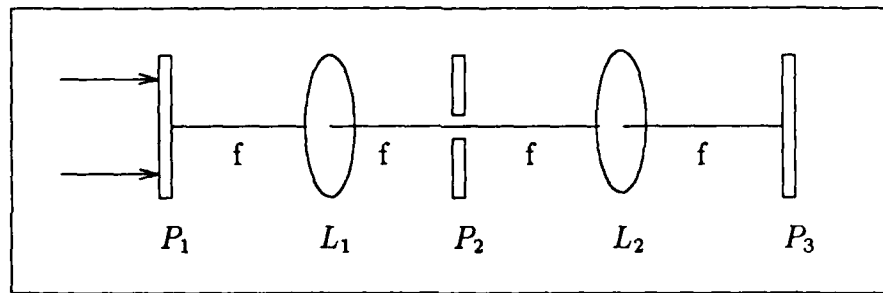


Figure 3. Optical Wavefront Generator

(13:128-129). This can be derived as follows. First, the two-dimensional FT of a shifted function is given by (9:313):

$$\mathcal{F}\{t(x - x_0, y - y_0)\} = e^{-j2\pi(x_0u + y_0v)} T(u, v) \quad (23)$$

Also (9:317),

$$\mathcal{F}\{\text{rect}(x, y)\} = \text{sinc}(u, v) \quad (24)$$

where (9:45)

$$\text{sinc}(u, v) = \frac{\sin(\pi u)}{\pi u} \frac{\sin(\pi v)}{\pi v} \quad (25)$$

The FT of a scaled function is (9:313)

$$\mathcal{F}\left\{t\left(\frac{x}{b}, \frac{y}{d}\right)\right\} = |bd| F(bu, dv) \quad (26)$$

Applying equations 23 through 26 to equation 22 yields,

$$T(u, v) = \sum_{n=1}^N \sum_{m=1}^M \frac{\sin(\pi w u)}{\pi u} \frac{\sin(\pi h_{mn} v)}{\pi v} e^{-j2\pi(nd_x u + md_y v)} \quad (27)$$

Due to the sampled nature of the CGH, this transform is periodic. Without the spatial filter, the second FT would result in an image of the CGH in plane P_3 . The spatial filter in plane P_2 passes only one order of the transform. This serves to remove the periodic, sampling information from the wavefront. The second FT produces the desired wavefront in plane P_3 .

In order to make it easy to pass only one order of the FT, the orders need to be separated by a convenient amount. This is where the sample spacing comes into play. For an object with transmittance $t(x, y)$ placed in the front focal plane of a FT lens, the wavefront at the back focal plane of the lens is given by

$$\mathcal{U}_f(x_f, y_f) = \int_{-\infty}^{\infty} \int_{-\infty}^{\infty} t(x_0, y_0) e^{-j\frac{2\pi}{\lambda f}(x_0 x_f + y_0 y_f)} dx_0 dy_0 \quad (28)$$

The amplitude of the light at (x_f, y_f) in the FT plane is related to the amplitude of the object spectrum at frequencies of $(\frac{x_f}{\lambda f}, \frac{y_f}{\lambda f})$ (10:86). To separate the orders and allow use of a convenient size spatial filter, the following equations must be evaluated for x_f and y_f :

$$f_x = \frac{x_f}{\lambda f} \quad \text{and} \quad f_y = \frac{y_f}{\lambda f} \quad (29)$$

where f is the focal length of the FT lens. For a periodic input object, $f_{x_0} = 1/U_x$, where U_x is the sample spacing in the x direction. Therefore,

$$x_{f_0} = f_{x_0} \lambda f = \lambda f / U_x \quad (30)$$

A spatial filter of diameter x_{f_0} is required to pass one FT order. This requirement can be controlled by the sample spacing and the focal length of the FT lens.

After the holograms are produced, the moments can be calculated. The Euclidean distance between the moment vectors can be used for pattern recognition. This method is described in the following section.

Euclidean Distance

A vector of dimension M can be plotted as a point in M space. The distance between two vectors can be found by calculating the distance between the two points. For two vectors, x and y , of dimension M , the Minkowski distance, M_N , is calculated by the following formula (12):

$$M_N = \sqrt[N]{\sum_{i=1}^M |x_i - y_i|^N} \quad (31)$$

where N is an integer. M_N is called the Taxi distance when $N = 1$, and the Euclidean distance when $N = 2$. A two-dimensional example is given in Figure 4. Here, the

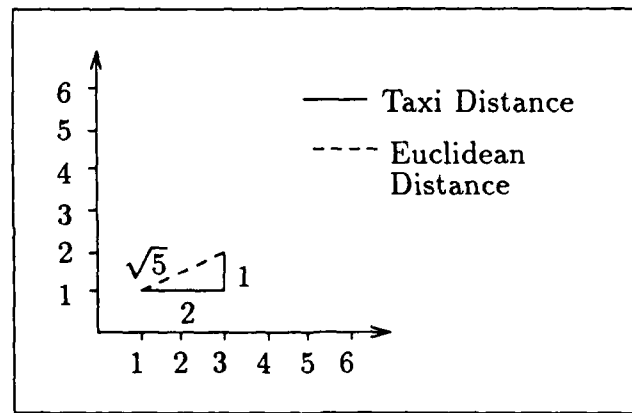


Figure 4. Distance Example

Taxi distance is:

$$M_1 = (3 - 1) + (2 - 1) = 3 \quad (32)$$

and the Euclidean distance is:

$$M_2 = \sqrt{(3 - 1)^2 + (2 - 1)^2} = \sqrt{5} \quad (33)$$

As long as the distance between the points is large enough to maintain separation when noise is added to the vectors, this system can be used for pattern recognition. That is, a set of points can be located for known objects, and the distance to

each of these points from an unknown vector calculated. The smallest distance will determine the classification of the unknown object.

This chapter explained how ordinary moments can be used to describe an object. These moments were then mathematically manipulated to form a PSRI set of moments. A setup to optically compute the ordinary moments was described, along with a method for generating amplitude holograms. Finally, the Euclidean distance method of pattern recognition was described. Chapter III details the production of the holograms, the experimental setup used to test their accuracy, and the data collection.

III. Procedures

The experimental portion of this research was carried out in three distinct steps. The first section of this chapter details the production of the computer generated holograms and the object transparencies. The second explains the experimentation conducted to ensure the holograms produced the desired wavefronts. Finally, the collection of the moments of the six objects is detailed in the third section.

Transparency Production

Before any data could be collected, the hologram and object transparencies had to be produced. The holograms were plotted using the computer program given in Appendix A. Since the final product was produced through photoreduction, the photographic negative of the hologram was printed from a laser printer onto an ordinary overhead transparency. The resultant plot for x is shown in Figure 5. Note that the heights of the rectangles increase linearly with distance. The resolution of the plotter resulted in the maximum height being attained approximately 14 cells before the edge. The remainder of the plots are shown in Appendix C.

In order to obtain a convenient separation of the FT orders, the program printed 100×100 cells in a 19.6×19.6 cm area. The transparency was photoreduced 20 times; (Appendix B), resulting in a 1×1 cm hologram with a sample spacing of 0.1 mm. The experimental optical system used a HeNe laser and a FT lens with a focal length of 101.6 cm. Using equation 30, the FT orders are separated by

$$x_{fo} = \frac{(630nm)(101.6cm)}{0.1mm} = 6.4mm \quad (34)$$

(This distance was 6.45 mm in the experimental setup.) With this separation, a standard iris could be used as the spatial filter.

The first four moment orders were calculated for the six sample objects. Since the holograms produced a wavefront which varied as a function of distance along an

axis, the same hologram could be rotated to provide variations in both the x and y direction. Therefore, it was necessary only to produce the following holograms: x , x^2 , xy , x^2y , and x^3 . (The zeroth order moment does not require a hologram, but only a square aperture of the appropriate size (1×1 cm)).

The object transparencies were then produced. Since the images were assumed to be segmented before the moments were calculated, the six objects were cut from rubylith and photoreduced onto glass plates in the same manner as were the holograms. The object masks varied in size, ranging from 1.6 cm for the plane to 0.7 cm for the tank.

After the appropriate masks were produced, the experimentation began. The first step was to ensure that the holograms would produce the desired wavefronts.

Hologram Tests

As explained in Chapter II, the desired wavefront was obtained by taking the FT of the FT of the hologram and blocking all but one order in the first FT plane. The experimental setup is shown in figure 6. The nominal focal length of the FT lens was used as a starting point for the setup. The exact position of planes P_2 and P_3 were found visually. A transparency of relatively large rectangles was placed at plane P_1 . The position of plane P_2 was pinpointed by following the beam with a white card. The spatial filter was positioned to pass the baseband of the FT.

Since the FT of the FT produces an image, the spatial filter was removed and the camera positioned to get the best focused image of the transparency on the monitor. This image was located at plane P_3 .

Once the setup was completed, the holograms were tested for accuracy. Each hologram was centered in the collimated beam (the most uniform area of the beam) at plane P_1 . To obtain consistency, each hologram had to be placed at the same spot in the beam. In order to do this, an alignment card was designed. A circle corresponding to the beam was drawn on one side of an index card. A 1×1 cm

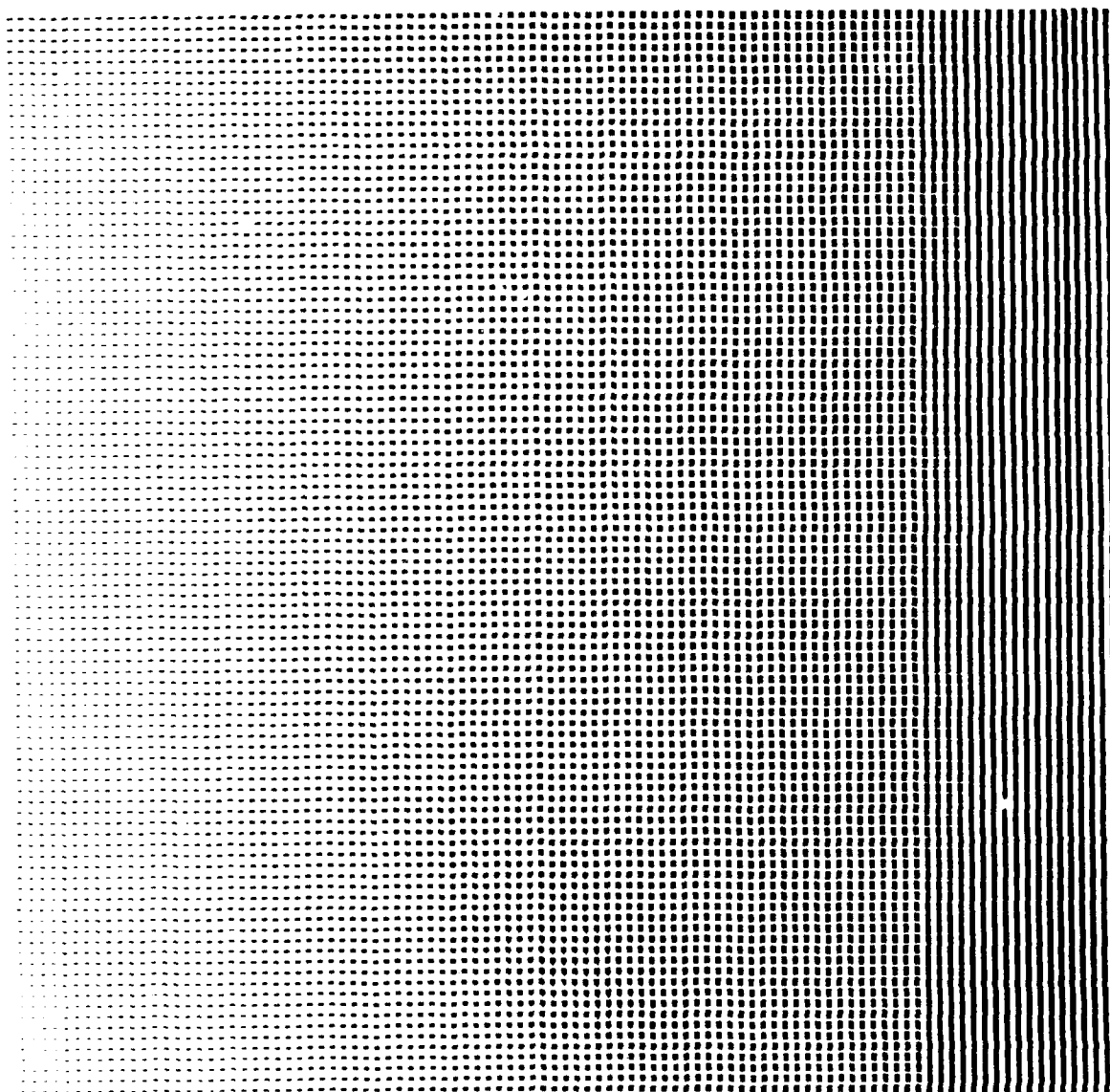


Figure 5. x CGII: Linear Ramp in Intensity

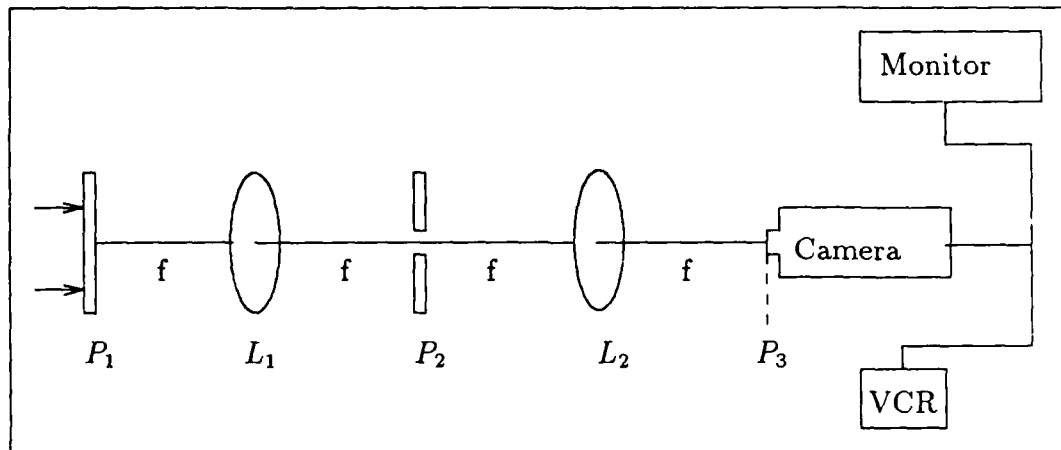
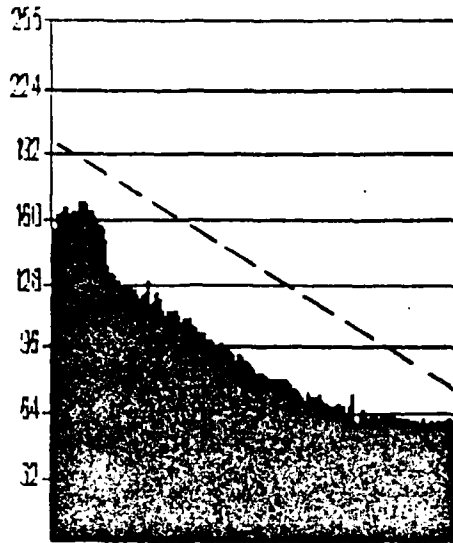


Figure 6. Computer Generated Hologram Test Setup

square was drawn, centered in the circle, on the other side of the card (Figure 9). The card was placed in front of the hologram, aligned with the square. The hologram was then moved until the circle was aligned with the beam. When both the square and the circle were lined up, the hologram was centered, and the card removed.

The wavefront produced at plane P_3 was recorded onto a VCR and taken to a frame grabber system for analysis. The Image-Pro software by Data Translation, Inc. was used to perform an intensity line profile at various positions along the wavefronts; sample outputs are shown in Figures 7 and 8. An area of constant high intensity was on the wavefront. This was a direct result of the threshold of the printer and was expected from the hologram (Figure 5). The center portion of the wavefront was linear (Figure 7). Since the objects were centered in the wavefront, the result was acceptable. The only object affected by the anomalies was the airplane, since it spanned nearly the entire magnified wavefront (see below) in the horizontal direction. Figure 8 shows that the wavefront was of a constant intensity, except for some noise, along a given profile in the y direction. Since the hologram varied in x , this was expected. There was a slight Gaussian shape due to the laser beam incident on the hologram.



*NOTE: Dashed line represents the desired profile.

Figure 7. Resultant Wavefront From "x" CGH - x Direction

The wavefront at plane P_3 was approximately 0.6×0.6 cm. In order to enlarge the wavefront to cover the objects, a magnifying lens was placed in the system past plane P_3 . The plane of the magnified wavefront was found by imaging a transparency, as was done to find plane P_3 . The resultant wavefront was 1.8×1.8 cm. Once this was accomplished, the moments could be calculated.

Moment Calculation

In order to calculate the ten moments needed for pattern recognition, the objects had to be placed in the same area of each wavefront. During the experiment, this requirement was fulfilled by centering each object. To ensure reproducibility, another alignment card was fabricated. A square corresponding to the size of the wavefront was drawn on an index card, with lines then added connecting the midpoints of opposite sides (Figure 9). The card was placed behind the plane of the magnified wavefront (P_4) and aligned with the wavefront (Figure 10). The object was then placed at plane P_4 so that the light passing through the transparency

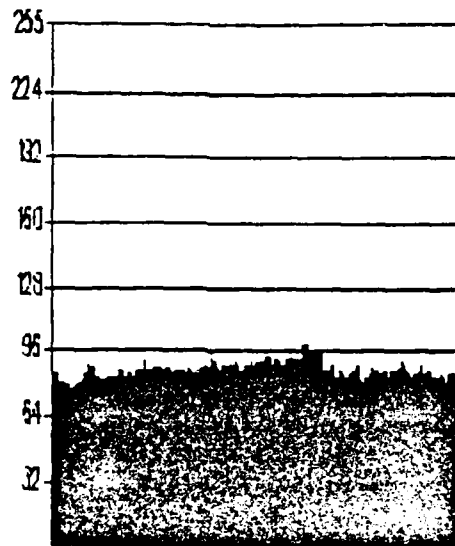


Figure 8. Resultant Wavefront From "x" CGH - y Direction

was centered on the card. The exact position of the moment space, plane P_6 , was determined by placing a square at plane P_4 and locating the sinc function on the camera.

In order to record all of the moments with a single camera, neutral density filters were placed at plane P_5 . A variable beam-splitter and Newport Corporation 835 Optical Power Meter were used to monitor beam changes.

Data Collection

The large dynamic range in intensities occurring at plane P_6 made it necessary to place neutral density filters at plane P_5 . This allowed control of the intensities sensed by the camera and, ultimately, by the Image-Pro software. A variable beam-splitter and power meter were used to monitor changes in the beam. To obtain the object moments, the setup shown in Figure 11 was used. To ensure that the waveform used for calculations was acceptable, the holograms were centered at plane P_1 , and the wavefront at plane P_3 was recorded onto the VCR. The camera was then moved to plane P_6 , and the six objects sequentially centered at plane P_4 . The

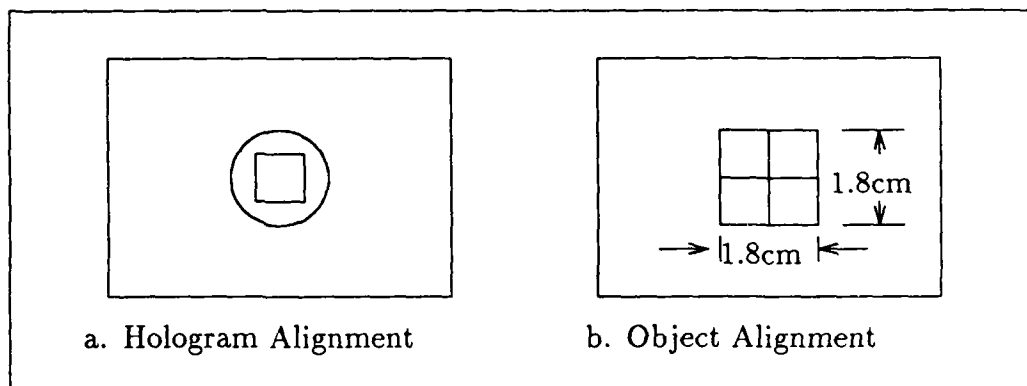


Figure 9. Alignment Card

resultant intensity pattern at plane P_6 was recorded onto the VCR. For each moment recorded, power meter readings of the beam were noted both before and after the neutral density filters were placed in the beam. (The filtering varied depending on the moment, and was experimentally gauged through an observation of the intensities on the monitor).

After all the data were recorded, the tape was taken to the frame grabber system for analysis. Using the Image-Pro software, the line profiles of the wavefronts were recorded. Appendix D contains this data. For each moment, the intensity pattern was thresholded to remove the background intensities, and the image scaled up in size. A schematic of a thresholded, scaled pattern is shown in Figure 12. It is a blocked pattern due to the pixels of the framegrabber. The center pixel is:

$$c(x, y) = \left(\frac{x_2 - x_1}{2}, \frac{y_2 - y_1}{2} \right) \quad (35)$$

where x_1 , x_2 , y_1 , and y_2 are the extreme points on the intensity pattern (Figure 12). Using the "histogram of a point" utility of the Image-Pro software, the center point was located and the intensity value recorded. The latter number was used to determine the moment value.

The power meter readings were in units of μW . The units of the intensity readings of the Image-Pro software is unknown. However, a scale factor would make

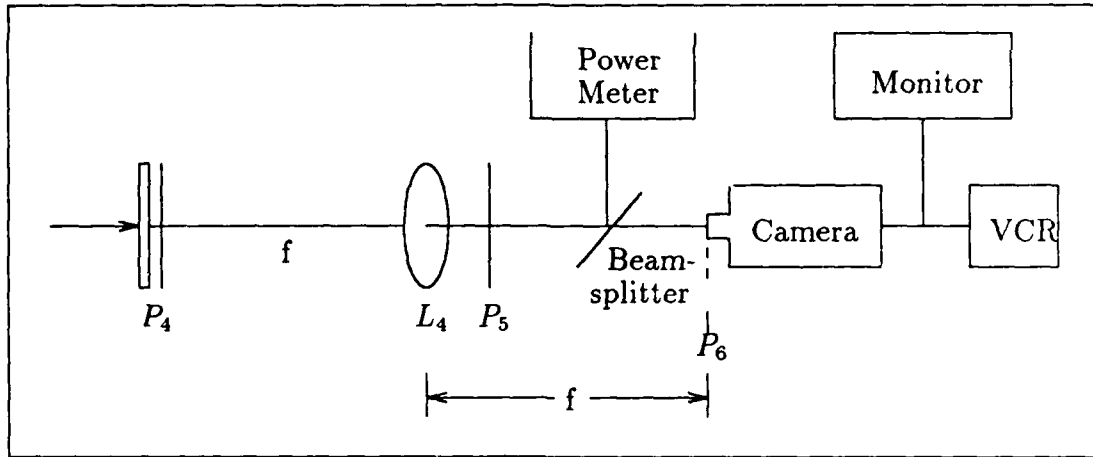


Figure 10. Moment Generation Setup

the intensity readings usable. (Since relations between the moments is the premise of this study, a scale factor will not affect the results). Therefore, the intensity readings were assumed to be in nW .

The moment value is a combination of the power meter readings and the intensity pattern midpoint. In order to determine the relationship, the effect of the neutral density filters and the beam-splitter had to be considered. The beam-splitter directed a portion of the energy into the power meter detector with the remainder entering the camera. The neutral density filters removed energy from the beam. Using Figure 13, the following relationships were developed:

$$I'b = P_a \quad (36)$$

$$I'(1 - b) = i = I' - I'b = I' - P_a \quad (37)$$

$$I' = i + P_a \quad (38)$$

$$b = \frac{P_a}{I'} = \frac{P_a}{i + P_a} \quad (39)$$

$$Ib = P_b \quad (40)$$

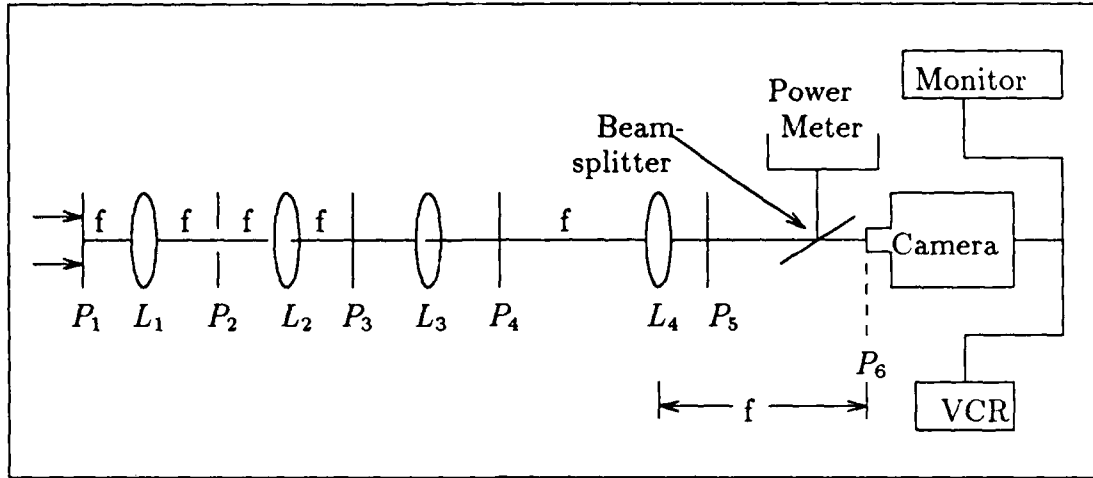


Figure 11. Experimental Setup

$$I = \frac{P_b}{b} = \frac{P_b}{P_a/(i + P_a)} = \frac{P_b(i + P_a)}{P_a} \quad (41)$$

Since every point on the beam was identically affected by the beam-splitter and the filters, the actual intensity of the moment was:

$$M = \frac{P_b(m + P_a)}{P_a} \quad (42)$$

where m was the value of the midpoint of the intensity pattern.

This chapter explained the experimental setup and procedures used to collect the data needed to find the moments of the six test objects. The procedures included the production and testing of the CGHs, and the recording of the intensity pattern in the moment plane. The method used to find the actual moment value from this data was discussed. Once the data was collected, it was tested for pattern recognition applicability. The next chapter details this process.

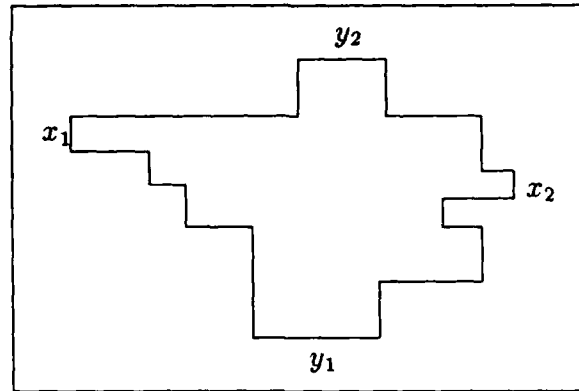


Figure 12. Thresholded, Scaled Intensity Pattern

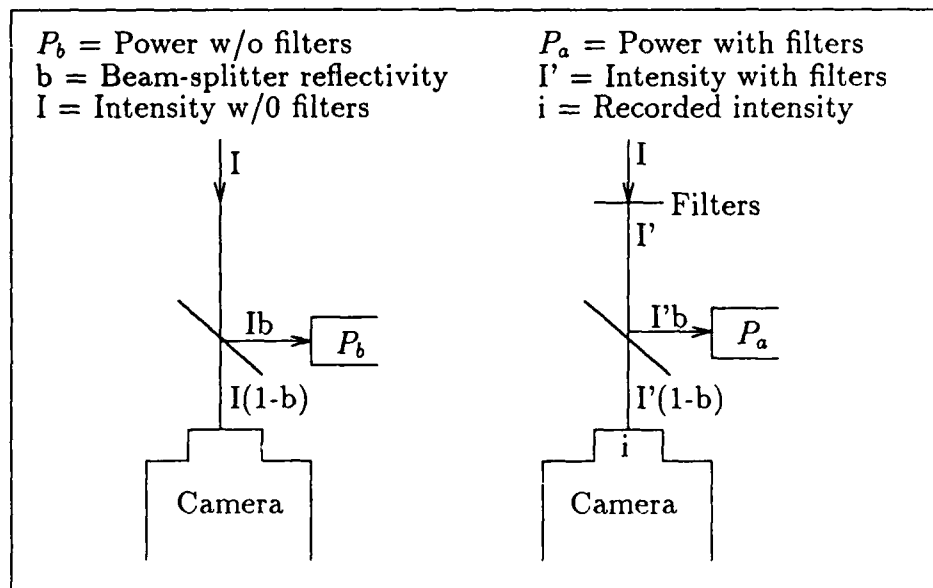


Figure 13. Effect of Optical System on the Beam

IV. Data Analysis

The moments of the six objects, up through the third order, were determined by the procedures described in Chapter III. The data analysis is contained in the current chapter. First, the ordinary moments are determined and the PSRI moments calculated. Section two contains an explanation of the Euclidean distance and its use in pattern recognition. Both the ordinary moments and the PSRI moments are tested for pattern recognition success. The results of these calculations are then discussed and analyzed for accuracy in section three.

Moment Values

The recorded data are shown in Table I. The power meter readings were not stable, as indicated by the \pm variations.

Equation 42 shows that the minimum moment value uses the minimum value of P_b and the maximum value of P_a . The maximum moment value was calculated using the maximum value of P_b and the minimum value of P_a . Table 2 contains the maximum, nominal, and minimum value for each of the moments.

The PSRI moments were calculated using equations 2, and 9-16. Again, there are three values for each moment of each object. The BASIC computer program used to perform these calculations is given in Appendix E, and the results provided in Table 3. The "min", "nom", and "max" labels refer to the ordinary moments used in the calculations. After the moment values were determined, the pattern recognition process was tested. The method used in this thesis was the Euclidean distance between vectors.

Distance Calculations

In this thesis, the vectors were composed of the moments of the objects. The Euclidean distances between the nominal vectors and all other vectors were calcu-

lated. The computer program for making the distance calculation is given in Figure 14. The distances for the ordinary moments are provided in Table 4, and those for the PSRI moments are shown in Table 5. The distances in Tables 4 and 5 were analyzed to provide an insight as to the feasibility of using this system for pattern recognition.

Results

Assuming the minimum and maximum vectors resulting from experimental uncertainties are representative of differences which would occur in the data, the distances in Tables 4 and 5 can be used to predict system accuracy. The distance from the nominal value to itself was zero, as expected. An error occurred for every one of the remaining values in the column which was less than the values for the distances to the minimum and maximum of the given object. (The errors are indicated by an asterisk in Tables 4 and 5.)

Using these criteria, the overall accuracy was calculated with the following formula:

$$\%correct = \frac{\#correct}{total\#} = \frac{total\# - \# of errors}{total\#} \quad (43)$$

Only six errors occurred out of 90 calculations using the ordinary moments, resulting in an accuracy of 93.3% (Table 4). With PSRI moments, the accuracy increased to 95.5% (Table 5). Further investigation revealed that every distance value from the circle to the square was less than that for the minimum and maximum values of the square. Thus, there was a high probability that this system would classify a square as a circle. This was not entirely surprising, however, since the square and the circle used were approximately the same size, and the only shape difference being a rounding of the corners. Thus, the low order moments would have been similar.

The data analysis was conducted in this chapter. After the ordinary and PSRI moment values had been calculated, the Euclidean distances between the objects

```

10 REM DATA MUST BE PLACED AT THE BEGINNING OF THIS PROGRAM
20 REM THIS PROGRAM USES 18 VECTORS WITH 10 ELEMENTS EACH
180 DIM DIST(18,18)
190 DIM A(18,10)
195 I = 1
200 FOR I = 1 TO 18
210 J = 1
220 FOR J = 1 TO 10
230 READ A(I,J)
240 NEXT J
250 NEXT I
260 U$="###.#"
270 N = 2
300 K = 1
310 FOR K = 1 TO 18
320 I = 1
330 FOR I = 1 TO 18
340 SUM = 0
350 J = 1
360 FOR J = 1 TO 10
370 B = (ABS(A(K,J) - A(I,J)))^ N
380 SUM = SUM + B
390 NEXT J
400 DIST(K,I) = SUM^ (1/N)
410 NEXT I
420 FOR S = 1 TO 9
430 LPRINT USING U$;DIST(K,S);
436 NEXT S
437 LPRINT " "
438 LPRINT
439 LPRINT
440 LPRINT
442 S = 10
443 FOR S = 10 TO 18
444 LPRINT USING U$;DIST(K,S);
445 LPRINT " ";
446 NEXT S
447 LPRINT " "
450 NEXT K

```

Figure 14. Distance Calculation Program

were found. There was a greater than 93% correct identification of the noisy objects.
The next chapter contains conclusions and some recommendations.

Table 1. Experimental Data

	m_{00}	m_{10}	m_{01}	m_{20}	m_{02}
Square					
P_b	$55.6 \pm .1$	$.68 \pm .01$	$.601 \pm .003$	$.107 \pm .002$	$.186 \pm .002$
P_a	$.018 \pm .002$	$.018 \pm .002$	$.017 \pm .002$	$.018 \pm .002$	$.019 \pm .002$
m	.194	.155	.190	.230	.122
Circle					
P_b	$41.7 \pm .1$	$.51 \pm .005$	$.415 \pm .003$	$.101 \pm .002$	$.095 \pm .001$
P_a	$.018 \pm .002$	$.018 \pm .002$	$.018 \pm .002$	$.018 \pm .002$	$.018 \pm .001$
m	.188	.180	.217	.200	.188
Triangle					
P_b	$19.9 \pm .1$	$.257 \pm .003$	$.110 \pm .001$	$.038 \pm .002$	$.026 \pm .002$
P_a	$.018 \pm .002$	$.018 \pm .002$	$.018 \pm .002$	$.018 \pm .001$	$.016 \pm .002$
m	.175	.170	.223	.175	.149
Truck					
P_b	$11.2 \pm .1$	$.126 \pm .002$	$.103 \pm .002$	$.027 \pm .001$	$.019 \pm .001$
P_a	$.018 \pm .002$	$.017 \pm .002$	$.018 \pm .001$	$.018 \pm .002$	$.017 \pm .001$
m	.138	.161	.147	.140	.143
Tank					
P_b	$9.9 \pm .1$	$.166 \pm .001$	$.067 \pm .002$	$.022 \pm .001$	$.019 \pm .001$
P_a	$.018 \pm .002$	$.016 \pm .001$	$.018 \pm .001$	$.018 \pm .003$	$.017 \pm .001$
m	.134	.158	.200	.167	.142
Plane					
P_b	$25.4 \pm .1$	$.402 \pm .003$	$.272 \pm .004$	$.107 \pm .002$	$.037 \pm .001$
P_a	$.018 \pm .002$	$.017 \pm .002$	$.017 \pm .002$	$.018 \pm .001$	$.018 \pm .002$
m	.124	.184	.143	.136	.115

This table is continued.

	m_{11}	m_{21}	m_{12}	m_{30}	m_{03}
Square					
P_b	$.098 \pm .001$	$.024 \pm .001$	$.024 \pm .002$	$.085 \pm .001$	$.019 \pm .001$
P_a	$.018 \pm .001$	$.018 \pm .001$	$.018 \pm .001$	$.019 \pm .001$	$.019 \pm .001$
m	.175	.141	.166	.114	.163
Circle					
P_b	$.045 \pm .001$	$.019 \pm .001$	$.022 \pm .001$	$.069 \pm .001$	$.054 \pm .001$
P_a	$.017 \pm .002$	$.018 \pm .001$	$.019 \pm .001$	$.019 \pm .001$	$.019 \pm .001$
m	.186	.170	.168	.126	.137
Triangle					
P_b	$.022 \pm .001$	$.024 \pm .001$	$.025 \pm .001$	$.039 \pm .001$	$.029 \pm .001$
P_a	$.018 \pm .002$	$.019 \pm .001$	$.020 \pm .001$	$.018 \pm .001$	$.018 \pm .001$
m	.154	.155	.188	.156	.138
Truck					
P_b	$.023 \pm .001$	$.022 \pm .001$	$.023 \pm .001$	$.042 \pm .001$	$.021 \pm .001$
P_a	$.018 \pm .001$	$.019 \pm .001$	$.019 \pm .001$	$.018 \pm .001$	$.018 \pm .001$
m	.125	.120	.145	.105	.106
Tank					
P_b	$.020 \pm .001$	$.021 \pm .001$	$.022 \pm .001$	$.029 \pm .001$	$.020 \pm .001$
P_a	$.018 \pm .001$	$.018 \pm .001$	$.019 \pm .001$	$.019 \pm .001$	$.018 \pm .001$
m	.154	.152	.150	.104	.126
Plane					
P_b	$.042 \pm .001$	$.031 \pm .001$	$.030 \pm .001$	$.091 \pm .001$	$.031 \pm .001$
P_a	$.018 \pm .001$	$.022 \pm .001$	$.021 \pm .001$	$.019 \pm .001$	$.018 \pm .001$
m	.134	.106	.155	.152	.122

Table 2. Ordinary Moments

	m_{00}	m_{10}	m_{01}	m_{20}	m_{02}	m_{11}	m_{21}	m_{12}	m_{30}	m_{03}
Square										
min	593.85	5.86	6.58	1.31	1.25	0.99	0.19	0.21	0.26	0.82
nom	654.84	6.54	7.32	1.47	1.38	1.05	0.21	0.24	0.60	0.87
max	731.06	7.37	8.25	1.68	1.54	1.12	0.23	0.23	0.63	0.93
Circle										
min	432.64	5.05	4.88	1.09	1.02	0.47	0.18	0.20	0.50	0.42
nom	477.23	5.61	5.42	1.22	1.09	0.54	0.20	0.22	0.53	0.44
max	532.95	6.31	6.09	1.39	1.16	0.62	0.22	0.24	0.56	0.47
Triangle										
min	193.05	2.41	1.32	0.37	0.22	0.18	0.20	0.24	0.35	0.23
nom	213.37	2.68	1.47	0.41	0.27	0.21	0.22	0.26	0.38	0.25
max	238.75	3.02	1.66	0.45	0.33	0.24	0.24	0.28	0.41	0.27
Truck										
min	87.69	1.17	0.88	0.21	0.16	0.17	0.15	0.18	0.27	0.13
nom	97.07	1.32	0.94	0.24	0.18	0.18	0.16	0.20	0.29	0.14
max	108.76	1.50	1.01	0.27	0.20	0.20	0.18	0.22	0.31	0.16
Tank										
min	75.46	1.70	0.75	0.19	0.16	0.17	0.18	0.18	0.17	0.14
nom	83.60	1.80	0.81	0.23	0.18	0.19	0.20	0.20	0.19	0.16
max	93.75	1.93	0.88	0.28	0.20	0.21	0.22	0.21	0.20	0.18
Plane										
min	182.16	4.26	2.28	0.86	0.24	0.33	0.17	0.23	0.77	0.22
nom	200.38	4.75	2.56	0.92	0.27	0.35	0.18	0.25	0.82	0.24
max	223.12	5.37	2.91	0.98	0.31	0.38	0.19	0.27	0.87	0.26

Table 3. PSRI Moments

	ϕ_1	ϕ_2	ϕ_3	ϕ_4	ϕ_5	ϕ_6	ϕ_7
Square							
min	7.11	30.25	0.00	0.02	0.00	0.11	0.00
nom	6.51	23.03	0.00	0.01	0.00	0.07	0.00
max	5.90	16.90	0.00	0.01	0.00	0.04	0.00
Circle							
min	11.02	24.21	0.00	0.05	0.00	0.26	0.00
nom	9.91	21.77	0.00	0.04	0.00	0.17	0.00
max	8.77	18.81	0.00	0.02	0.00	0.10	0.00
Triangle							
min	15.50	104.65	0.97	1.87	2.24	19.07	1.14
nom	14.63	90.44	0.70	1.34	1.17	12.75	0.56
max	13.41	72.12	0.47	0.89	0.53	7.56	0.24
Truck							
min	46.98	1903.58	31.56	50.36	1653.46	2091.11	1138.60
nom	43.52	1429.48	22.96	33.60	801.91	1282.75	626.62
max	38.80	1123.05	16.41	24.23	397.20	785.14	274.81
Tank							
min	59.42	3357.86	110.02	83.15	7916.16	4818.06	760.73
nom	56.77	2814.79	80.61	62.66	4437.30	3320.50	378.26
max	52.89	2217.30	52.31	41.34	1922.12	1921.41	-33.90
Plane							
min	31.77	680.05	0.38	5.06	6.83	131.64	1.50
nom	28.39	515.99	0.25	3.60	3.27	81.50	0.85
max	24.82	377.10	0.15	2.38	1.37	46.10	0.41

Table 4. Ordinary Moment Distances

	Square nom	Circle nom	Triangle nom	Truck nom	Tank nom	Plane nom
Square min	61.0	116.6	380.5	496.8	510.3	393.5
nom	0.0	177.6	441.5	557.8	571.3	454.5
max	76.2	253.9	517.8	634.1	647.5	530.7
Circle min	222.2	44.6	219.3	335.6	349.1	232.3
nom	177.6	0.0	263.9	380.2	393.7	276.9
max	121.9	55.7	319.6	435.9	449.4	332.6
Triangle min	461.9	284.2	20.3	96.0	109.5	*7.8
nom	441.5	263.9	0.0	116.3	129.8	*13.2
max	416.1	238.5	25.4	141.7	155.2	38.4
Truck min	567.2	389.6	125.7	9.4	*4.1	112.8
nom	557.8	380.2	116.3	0.0	13.5	103.4
max	546.1	368.5	104.6	11.7	25.2	91.7
Tank min	579.4	401.8	137.9	21.6	8.1	125.0
nom	571.3	393.7	129.8	13.5	0.0	116.8
max	561.1	382.5	119.6	*3.4	10.2	106.7
Plane min	472.7	295.1	31.3	85.2	98.6	18.2
nom	454.5	276.9	*13.2	103.4	116.8	00.0
max	431.7	254.1	*10.2	126.1	139.6	22.8

* ERROR

Table 5. PSRI Moment Distances

	Square nom	Circle nom	Triangle nom	Truck nom	Tank nom	Plane nom
Square min	7.25	8.93	61.99	2154.49	6214.84	493.00
nom	0.00	3.63	69.10	2159.22	6218.10	500.15
max	6.16	6.32	75.17	2163.25	6220.88	506.23
Circle min	*4.67	2.68	67.52	2158.27	6217.44	498.77
nom	*3.63	0.00	70.00	2159.92	6218.59	501.23
max	*4.79	3.18	73.00	2161.91	6219.97	504.21
Triangle min	84.34	85.25	15.63	2094.08	6169.92	416.26
nom	69.10	70.00	0.00	2107.50	6180.38	431.30
max	50.15	51.02	19.10	2122.66	6191.75	450.26
Truck min	3456.07	3456.66	3411.25	1365.94	*3266.84	3159.91
nom	2159.22	2159.92	2107.50	0.00	4399.26	1818.96
max	1435.82	1436.65	1377.05	793.26	5062.51	1046.25
Tank min	9879.29	9879.63	9849.49	8176.66	3845.47	9681.00
nom	6218.10	6218.59	6180.38	4399.26	0.00	5965.68
max	3494.09	3494.78	3444.34	1649.46	2968.45	3157.16
Plane min	670.60	671.69	601.76	1706.23	5874.29	171.62
nom	500.15	501.23	431.30	1818.96	5965.68	0.00
max	357.54	358.61	288.78	1916.18	6041.14	143.39

* ERROR

V. Conclusions and Recommendations

Conclusions

This thesis had several successes. The method to generate binary amplitude holograms was first researched and implemented. The resultant waveforms were close to the correct form. Anomalies occurred mainly near the edges, due to the method used to print the holograms. Recommendations for producing better holograms are given in the next section. Second, the moments of six objects were optically calculated. By using a beam-splitter and power meter, one camera could record all of the intensity patterns. Third, the PSRI moments were calculated by digital postprocessing. Finally, both the ordinary and PSRI moments were found to be separable, based on the calculated Euclidean distances.

The hybrid generation of a PSRI moment set appears to be useful. The data collected can be utilized for pattern recognition purposes, but a knowledge of the accuracy required for a given scenerio would dictate its applicability. Recommendations are given in the following section.

Recommendations

The conclusions are based upon only one set of data. For the given objects, all centered in the wavefront, the values are separable. Further investigation is needed to determine the accuracy of the system. Data should be taken for various scaled, rotated, and translated objects, and then compared with itself and the current data. An estimate of the accuracy could then be made.

The data analysis could be improved. Different Minkowski distances could be tested, since the Euclidean distance may not provide the best separation of the data. The PSRI moments could also be fed into a neural network. A multilayer perceptron

neural network would be able to find relations and differences in the data not used in the distance calculations.

An optical system could calculate the low order moments in both the space and frequency domains. The frequency domain moments would aid in distinguishing classes inseparable by general shape (8:1073).

The number of moments necessary to separate tactical targets needs to be investigated. Seven PSRI moments appeared to be adequate for the six objects investigated here. More may be required for distinguishing closely related objects.

The current optical system could be made more efficient. A spatial light modulator could be used in the object plane. With this device, the objects of interest could be quickly interchanged. By the appropriate use of phase, multiple CGHs could be recorded on one mask. This would allow the simultaneous computation of the ordinary moments. Also, having the framegrabber system and Image-Pro software in the same laboratory could save time. The use of a small optical detector would allow the ordinary moment values to be determined in real-time.

Finally, the CGHs could be improved. Ideally, the rectangles should be dark enough to block all the light during photoreduction. However, the print quality of the process used in the research was poor, and resulted in holograms which were not totally pass/no pass. A Hewlett Packard Jet laser printer might improve the print quality, but would require a new program for generating the CGH. Second, the number of cells printed resulted in areas of constant intensity, due to the printer threshold. This problem could be eliminated by determining the number of cells which could be used, so as to not have rectangles of constant height on either edge of the hologram. (The x^2 hologram appeared to be the worse case.) Since the final sample spacing helps determine the separation of the FT orders, a tradeoff should be made between the number of cells, the amount of reduction, and the focal length of the FT lens.

Incorporating these recommendations should result in an efficient, accurate pattern recognition process.

Appendix A. *Hologram Production*

The generation of the detour phase hologram is detailed in this Appendix. The program used to print the hologram is first presented. The variables used are then explained.

Program

The following program generates a detour phase hologram which will produce a wavefront with an amplitude of the form x^p, y^q .

```
Parameter (D=64, P=1, Q=0)
Call Setplot('bigx',1,0,.false.)
Call mapxy(0.,1.,0.,1.,0.,1.,0.,1.,0,1)
Do 30 m = 1, D
Do 20 n=1, D
hmag = ((m/D)**P) * ((n/D)**Q)
Call box (m,n,hmag)
20 Continue
30 Continue
Stop
End
C
Subroutine box(m,n,hmag)
Parameter (iboxw=35,iw=17,ihmax=35,iosx=500,iosy=90)
icx = m*iboxw - (iboxw/2) + iosx
icy = n*iboxw - (iboxw/2) + iosy
ih = ihmax * hmag
ilx = icx - (iw/2)
```

```

ily = icy - (ih/2)
Do 10 i = ilx, ilx + iw
Call drv(i,ily,i,ily+ih)
10 Continue
Return
End

```

Three METALIB program subroutines are used. The variables of the program are discussed in the following section.

Variables

The parameters needed to run this program are detailed below. The METALIB manual was used as a reference.

The first step is to determine the number of cells the hologram will contain. (This value depends on the sample spacing needed.) For this program, the hologram was square, with an equal number of cells in both the x and y direction. The variable "D" represents the number of cells in one direction. The variables P and Q are the powers of x and y, respectively. These three variables must be set by the programmer in line 1.

Next, the setplot and mapxy METALIB subroutines are called. These direct the printer on how to plot the output. Setplot has four parameters which must be specified, as shown in the generic example below.

Call Setplot('pltname', lunplt, lunmsg, .frameid.) (44)

The parameters are:

1. pltname: name of the output file. This name must be changed for each new plot. METALIB will not overwrite an existing file.

2. `lunplt`: output file logical unit number
3. `lunmsg`: logical unit number for plotting system error messages. For the UNIX system, zero is standard.
4. `frameid`: enables (true) or disables (false) a frame identification label. If "true", this label is printed on each output.

Mapxy has ten parameters which must be specified.

Call `mapxy(amin.,amax.,bmin.,bmax.,amii.,amaa.,bmii.,bmaa.,igrid,itype)`
(45)

The parameters are:

1. `amin,amax`: minimum and maximum values along the x axis, in user coordinates. Since the amplitude is normalized, the values used in this program are (0,1).
2. `bmin,bmax`: minimum and maximum values along the y axis, in user coordinates. From the same argument given above, the values used in this program are (0,1).
3. `amii,amaa,bmii,bmaa`: minimum and maximum values along the x and y axes, respectively, in absolute coordinates. This program uses the entire sheet of paper, so the values used are (0,1,0,1).
4. `igrid`: type of grid to be drawn. This program used "0" which results in no border, grid lines, or hash marks.
5. `itype`: the type of mapping to be used. This program uses a "1" which results in a linear, linear plot.

The next step is to compute the normalized amplitude for each (n,m) location along the wavefront. This value is assigned to the variable "hmag" and is computed in line 6 of the program.

The subroutine "box" draws the proper rectangle, based on $hmag$, at the center of each cell. In this subroutine, the following variables must be inserted by the user:

1. $iboxw$: number of pixels in each cell width
2. iw : number of pixels in each rectangle along the x direction
3. $ihmax$: maximum number of pixels in each rectangle along the y direction
4. $iosx$: number of pixels skipped along the x direction before printing begins
5. $iosy$: number of pixels skipped along the y direction before printing begins

The above numbers are determined as follows. The pixel dimensions for an entire sheet of paper are 3270×2445 pixels ($x \times y$). There is an automatic offset of 30 and 25 pixels in the x and y directions, respectively. The number of pixels in the y direction is used in the following calculations, since this direction has the fewest pixels. Follow the formula below to determine $ihmax$. Round the answer down in order to avoid addressing more pixels than are available. Also, using the nearest odd number will cause the rectangle to be printed exactly in the center of each cell.

$$ihmax \approx \frac{2445 - 25}{D} \quad (46)$$

In this program, each cell was square, so that $ihmax = iboxw$.

$$iw = \frac{1}{2}(iboxw) \quad (47)$$

To center the hologram on the paper, $iosx$ and $iosy$ are determined from the formulas below:

$$iosx = \frac{(3270 - D * iboxw) + 30}{2} \quad (48)$$

$$iosy = \frac{(2445 - D * ihmax) + 25}{2} \quad (49)$$

Due to equipment limitations, the edges of the paper did not print well. Therefore, the user may elect, as the programmer did, to not use all available pixels. This is accomplished by making $ihmax$ and iw , in the above equations, smaller.

Once these parameters are set, the center pixel of the cell (n,m) is located. This is accomplished in lines 3 and 4 of the subroutine "box". Line 5 computes the height of the rectangle which will be placed in this cell, centered on the pixel found above. The lower left hand corner of the rectangle is calculated in lines 6 and 7.

The rectangle is drawn by using the *drv* METALIB subroutine. The four parameters, described below, must be specified for this subroutine.

1. ix,iy: pixel coordinates for the beginning of the line
2. jx,jy: pixel coordinates for the end of the line

This subroutine is called in a "Do" loop which goes from the x coordinate of the lower left hand corner to the x coordinate of the lower right hand corner. The height of the rectangle, (iy,jy), remains constant for a given cell.

To compile this program on the ssc system at AFIT, use the command

```
f77 programname programname.f -lmetalib (50)
```

Run by typing the program name. The hologram is printed by using the command:

```
mit pltname | lpr - Pimagen.
```

Appendix B. *Photoreduction Process*

This appendix details the photoreduction process used to produce the CGH transparencies. The information presented here was obtained, in part, from the thesis presented in 1987 by Lt Mayo (14:83-84).

As discussed in chapter III, the negatives of the CGHs were printed onto overhead transparencies. Once this was completed, the transparencies were taken to the Cooperative Electronics Materials Processes Laboratory (room 1065) in building 125 to be photoreduced onto high resolution glass slides.

The Dekacon optical system, shown in Figure 15, was used to reduce the CGH and expose the glass plate. The manual for the system was consulted to determine the proper lens and box positions for the reduction required. For 20 \times reduction, the 3-in Wray lens was placed in the system, the front box set at position 6.88, and the rear box set at position 27.00. (The positions are read by placing a penlight in the hole of the position indicator.) This process will set the system at approximately the correct position.

To ensure the system was focused, a scratched glass plate was placed in the plate holder, and the transparency of the negative of the hologram taped to the object screen. The screen was back illuminated with green light. The shutter and rubyolith were removed from the plate holder, and a microscope positioned behind it so that the scratches on the plate were in focus. (The back box was moved to aid in this process.) The front box was moved until the rectangles of the CGH came into focus. When both the rectangles and the scratches were in focus, the system was focused. The scratched surface of the plate had to face the screen, since the emulsion of the high resolution glass plate faced in that direction. Once the system was focused, all settings were locked into place by tightening the four screws located on the positioners.

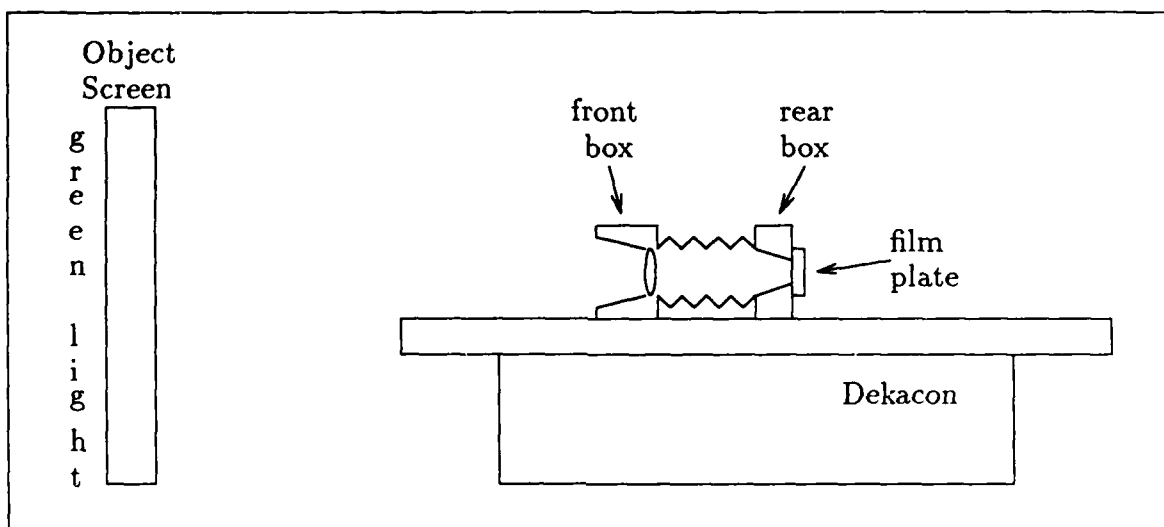


Figure 15. Dekacon Photoreduction System

Next, the scratched plate was removed, and the rubylith placed over the hole in the plate holder. A 2×2 inch high resolution glass slide was placed in the plate holder, with its emulsion side toward the screen. (The green light must be turned off when interchanging the glass plates. The emulsion was insensitive to red light, so this light was used for visual reference.) The plate was exposed for $2\frac{1}{2}$ to 3 minutes by removing and replacing the shutter. The exposed plate was developed for 4 to 6 minutes. The times varied, depending on the type and age of the developer. Good results were obtained by checking the darkness of the plate every few seconds after one minute. When the rectangles were visible, and the surrounding area was "dark", the plate was placed in the stop bath for 20 seconds. This was followed by one minute in the fixer and a rinsing in deionized water. This process was repeated for each hologram.

Appendix C. *CGH Plots*

This appendix contains the plots used to generate the holograms for this thesis. The program which produced the plots is contained in Appendix A.

The plots produced had areas of rectangles with constant height, due to the printer threshold. The intensity line profiles in Appendix D indicate that the resultant wavefronts were fairly accurate.

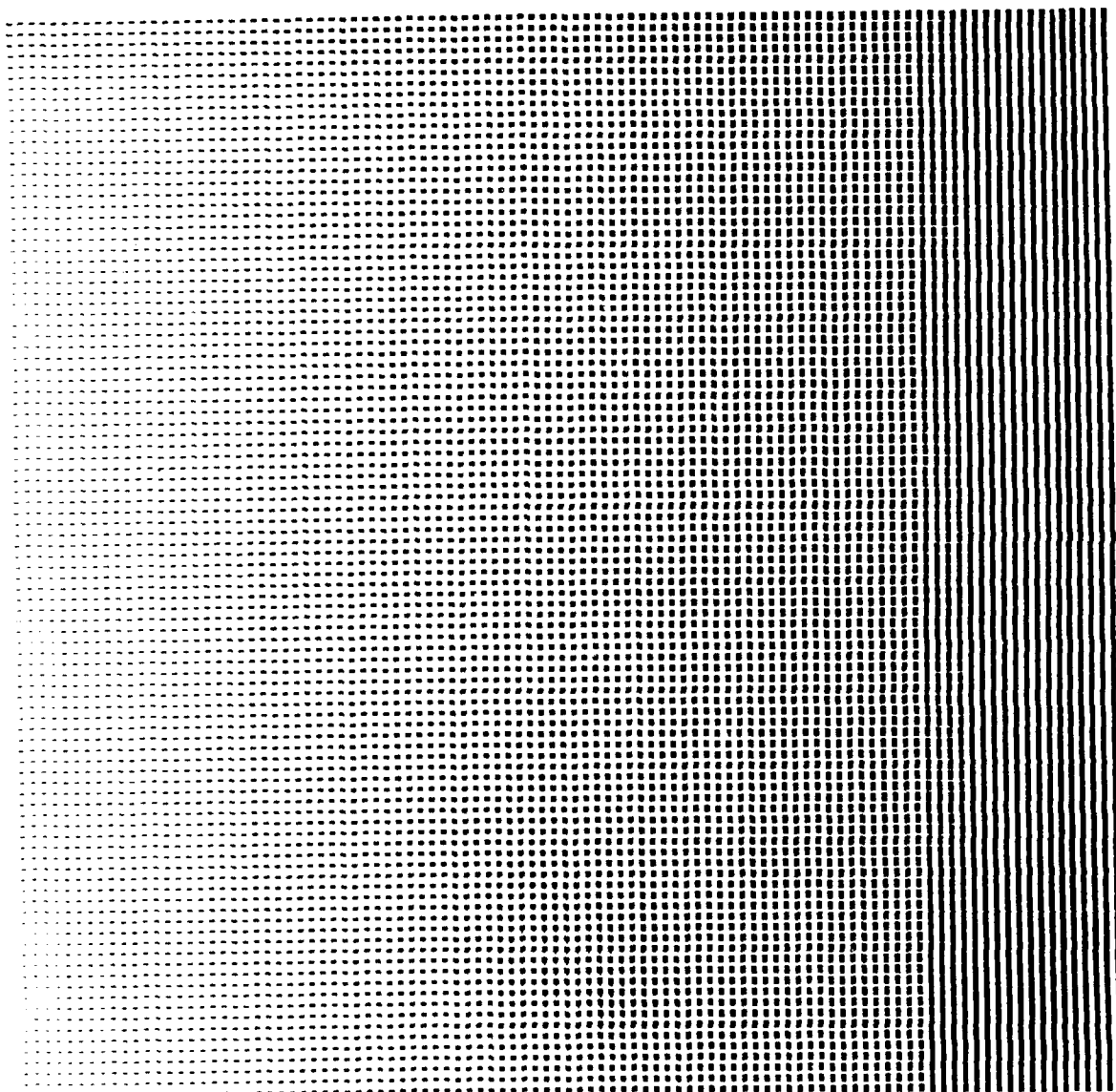


Figure 16. x CGH Plot

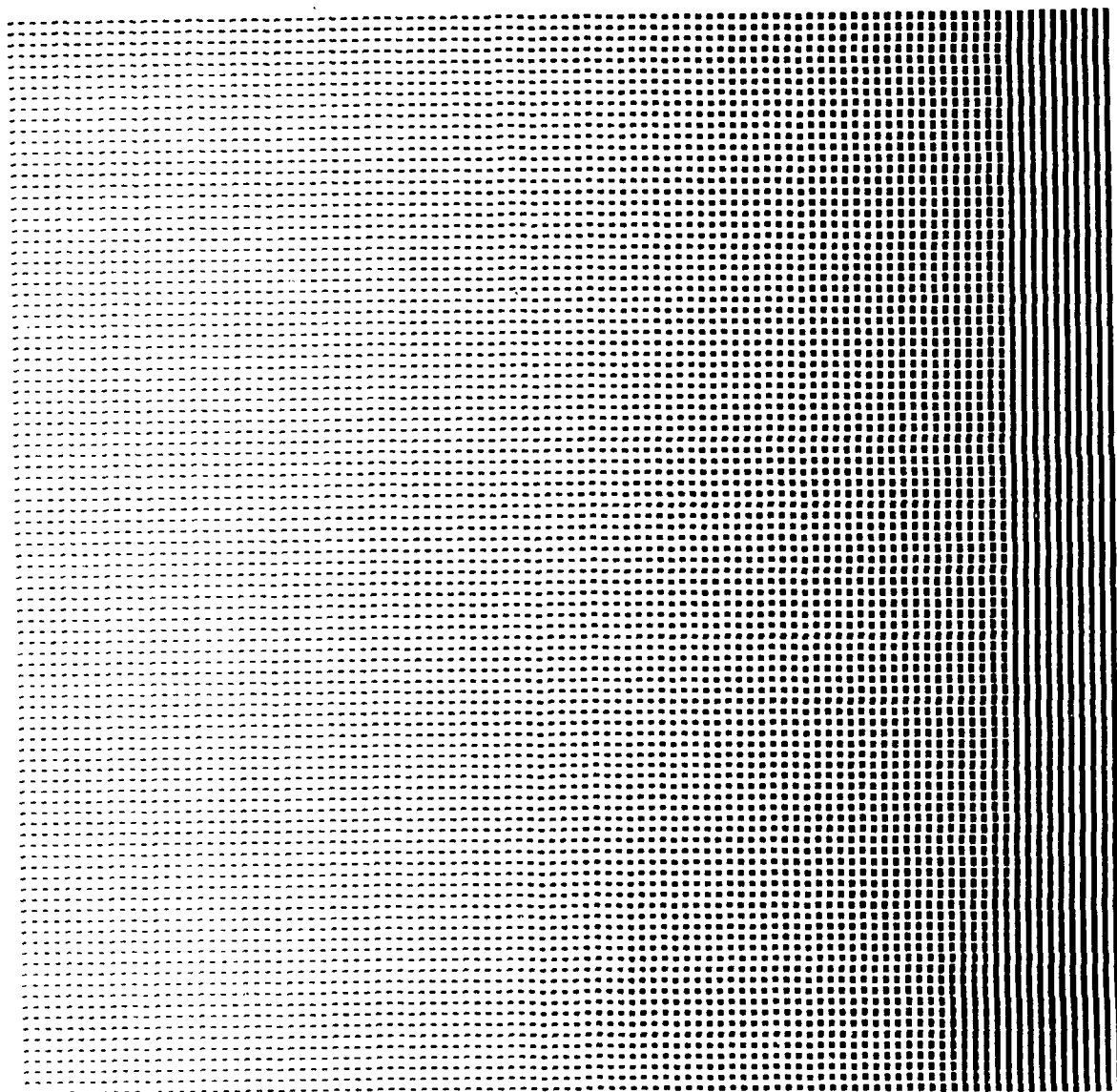


Figure 17. x^2 CGII Plot

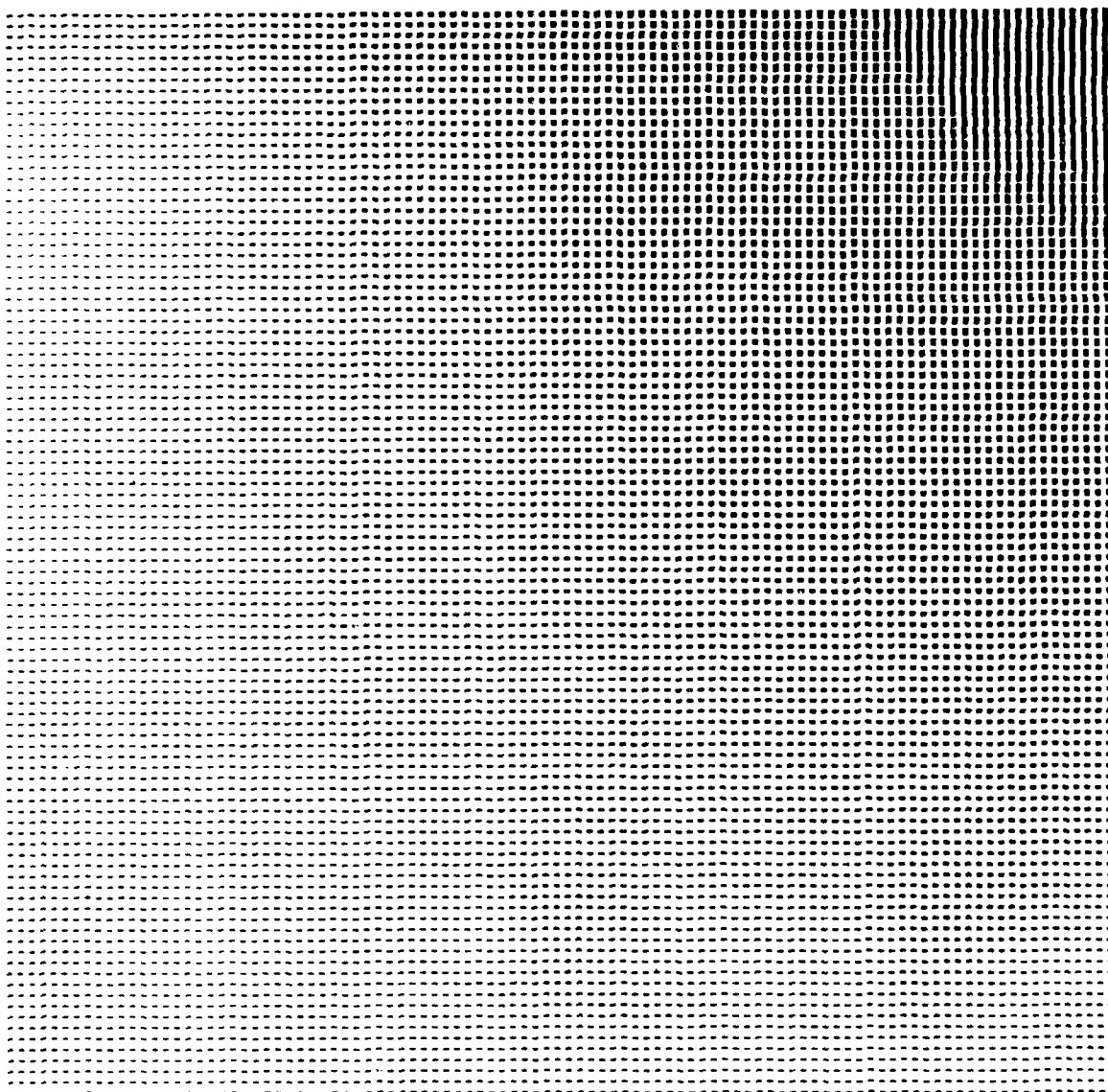


Figure 18. xy CGH Plot



Figure 19. x^2y CGH Plot

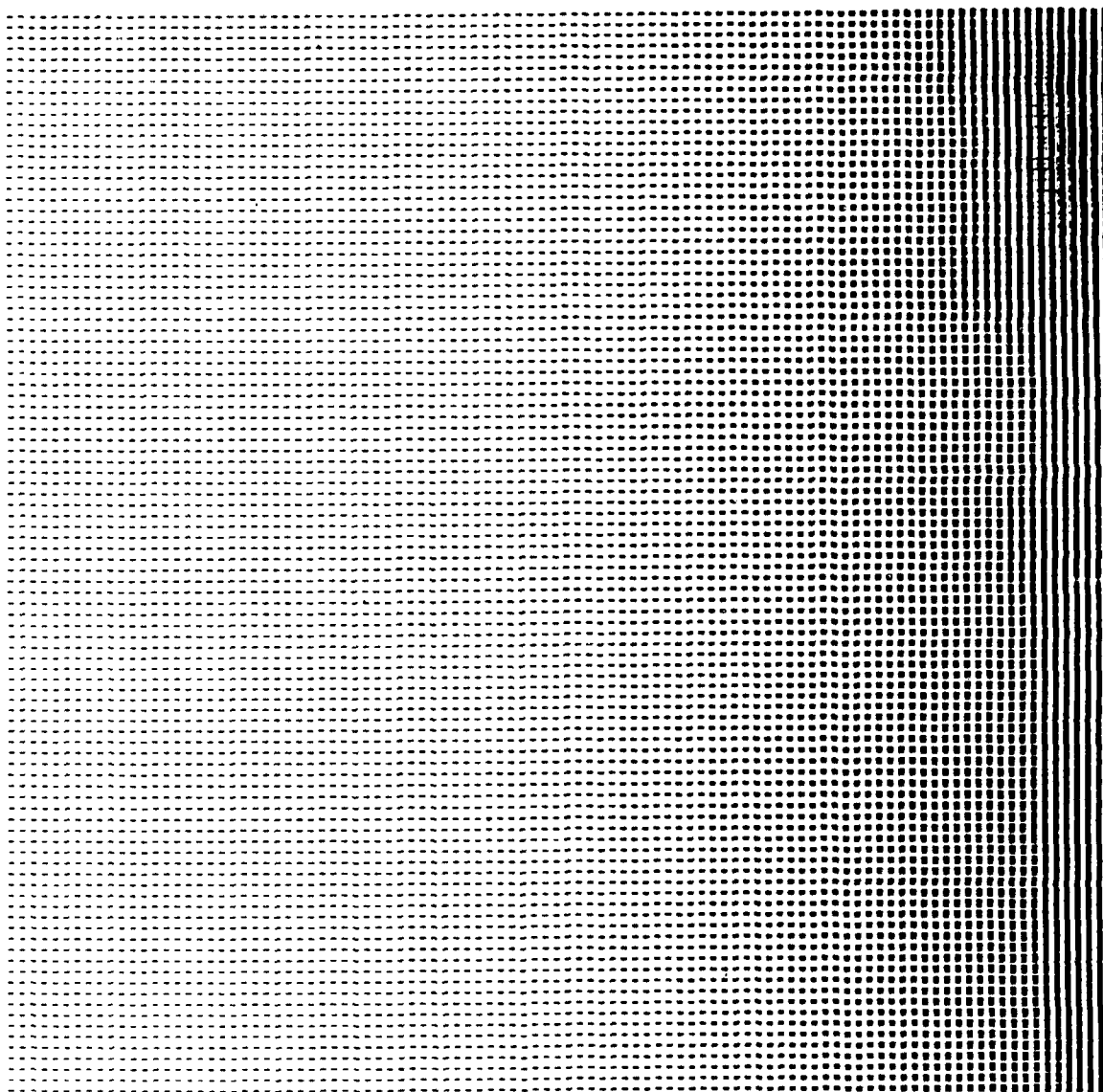


Figure 20. x^3 CGII Plot

Appendix D. *Intensity Line Profiles of the x^py^q Wavefronts*

This appendix contains the intensity line profiles taken to test the accuracy of the CGHs. The first figure for each wavefront indicates the approximate positions of the line profiles. The beam wavefront was recorded at the beginning and end of the data taking session to ensure that the profile had not changed significantly. Figures 21 and 27 indicate that the profile remained fairly consistent throughout the experiment.

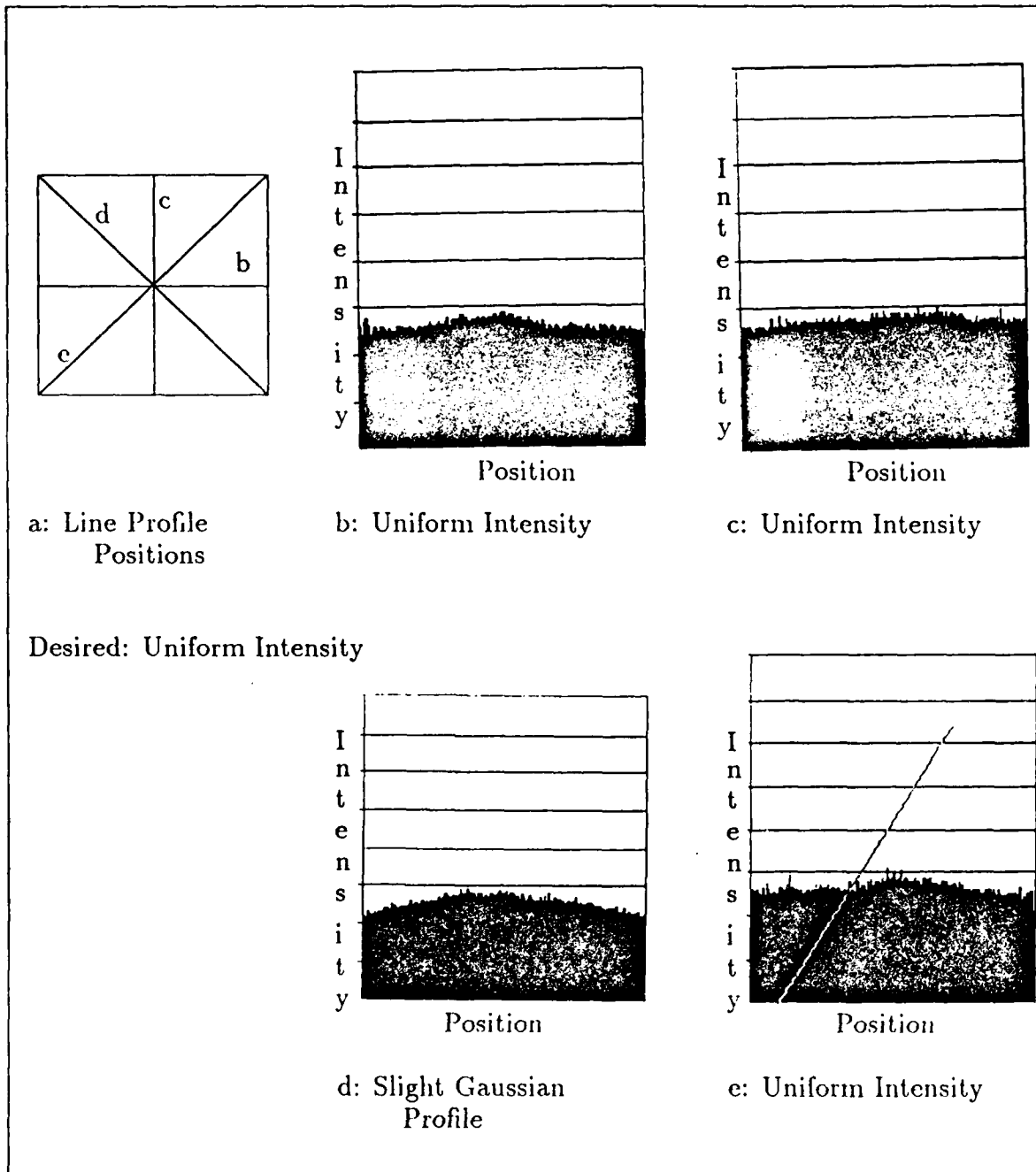


Figure 21. Beginning Beam Wavefront Profiles

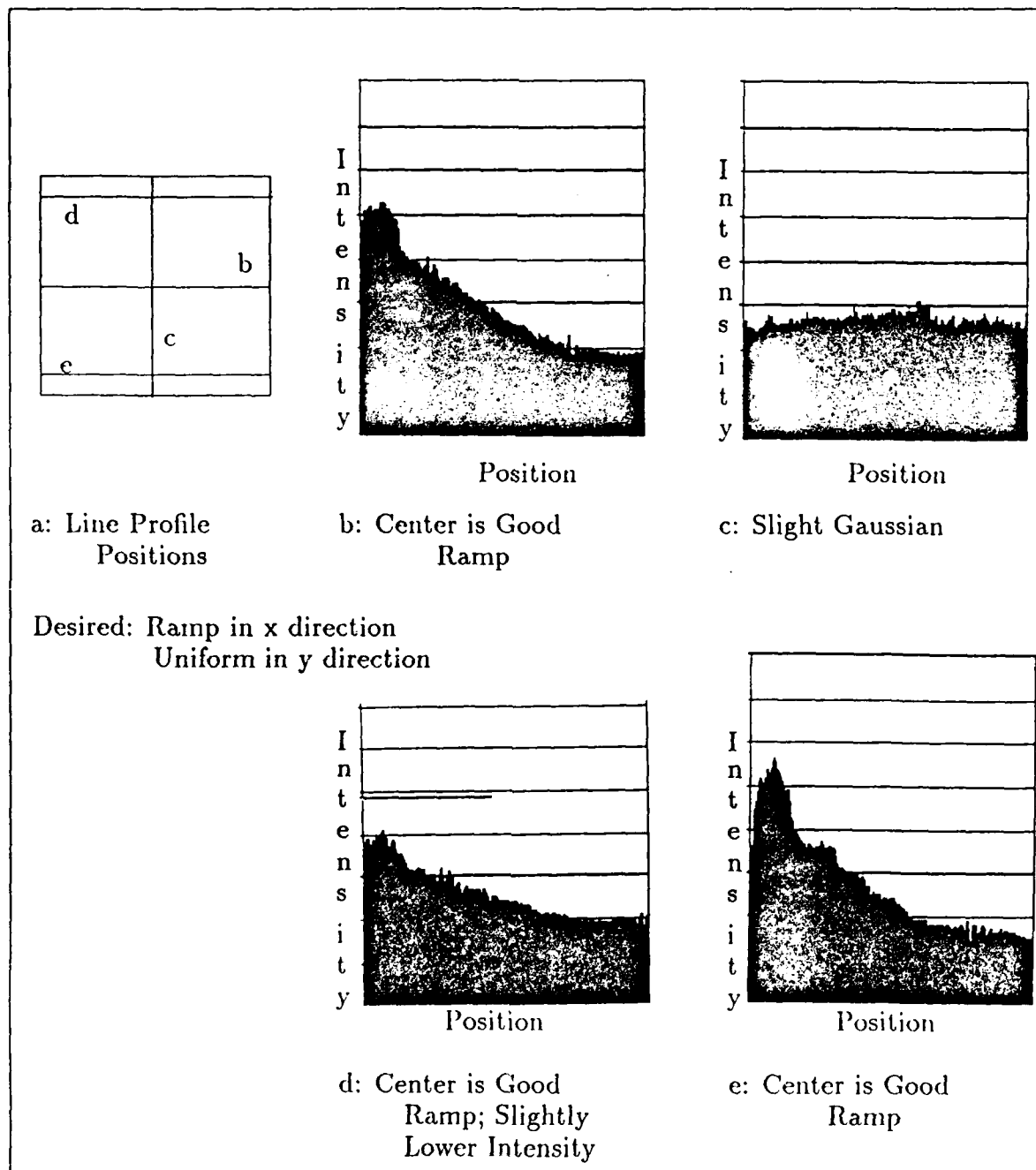


Figure 22. "x" Wavefront Profiles

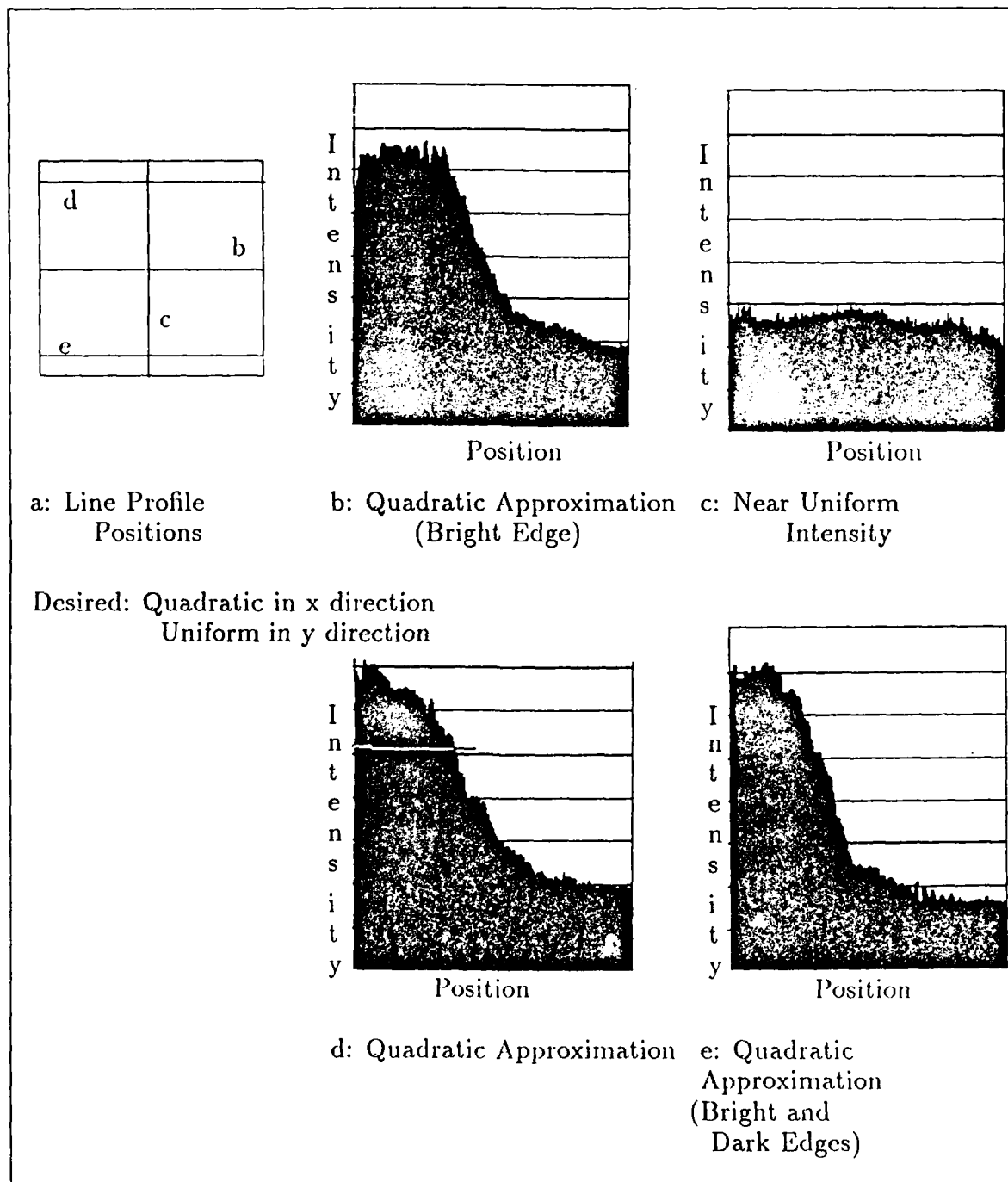


Figure 23. x^2 Wavefront Profiles

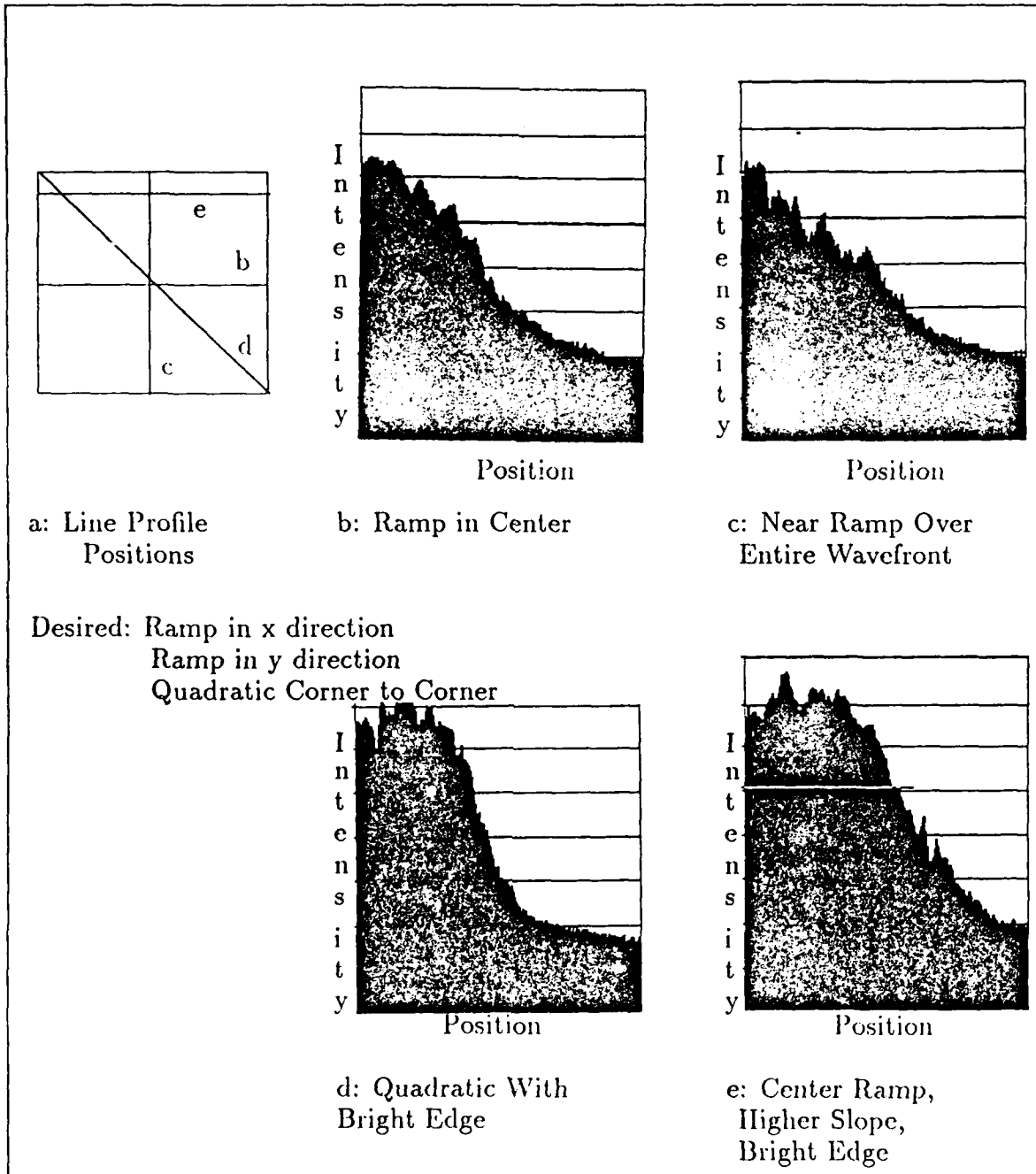


Figure 24. xy Wavefront Profiles

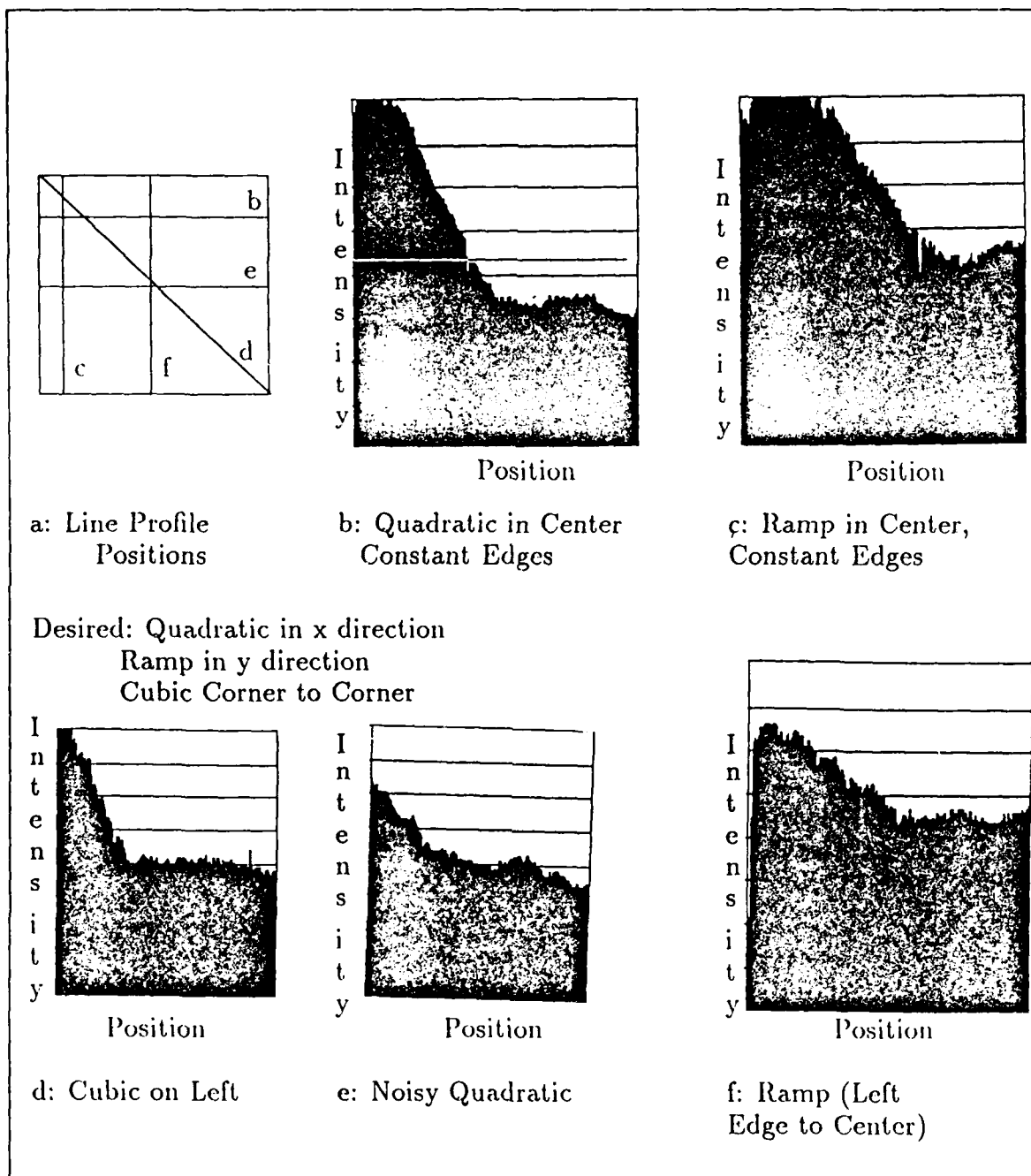


Figure 25. x^2y Wavefront Profiles

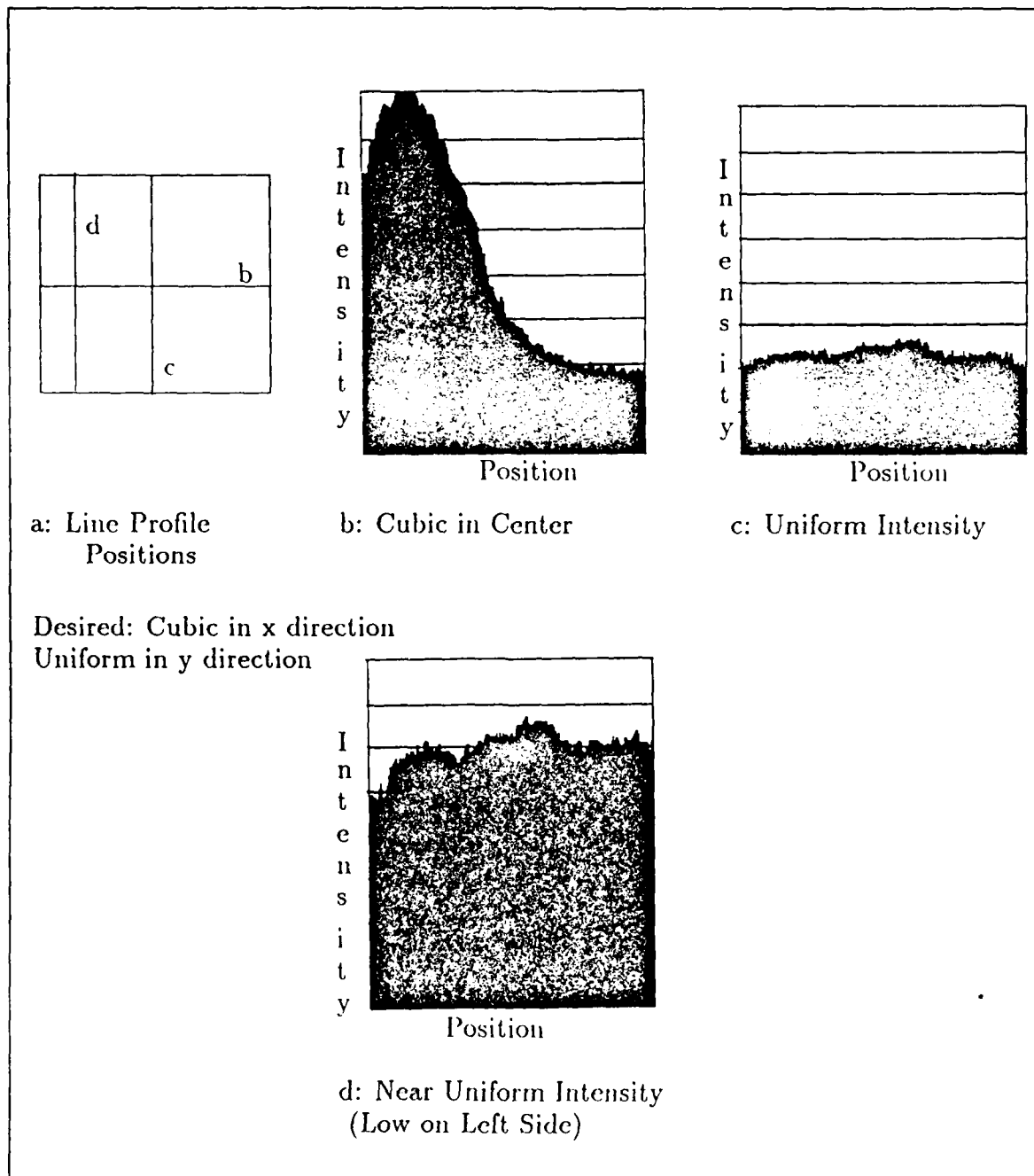


Figure 26. x^3 Wavefront Profiles

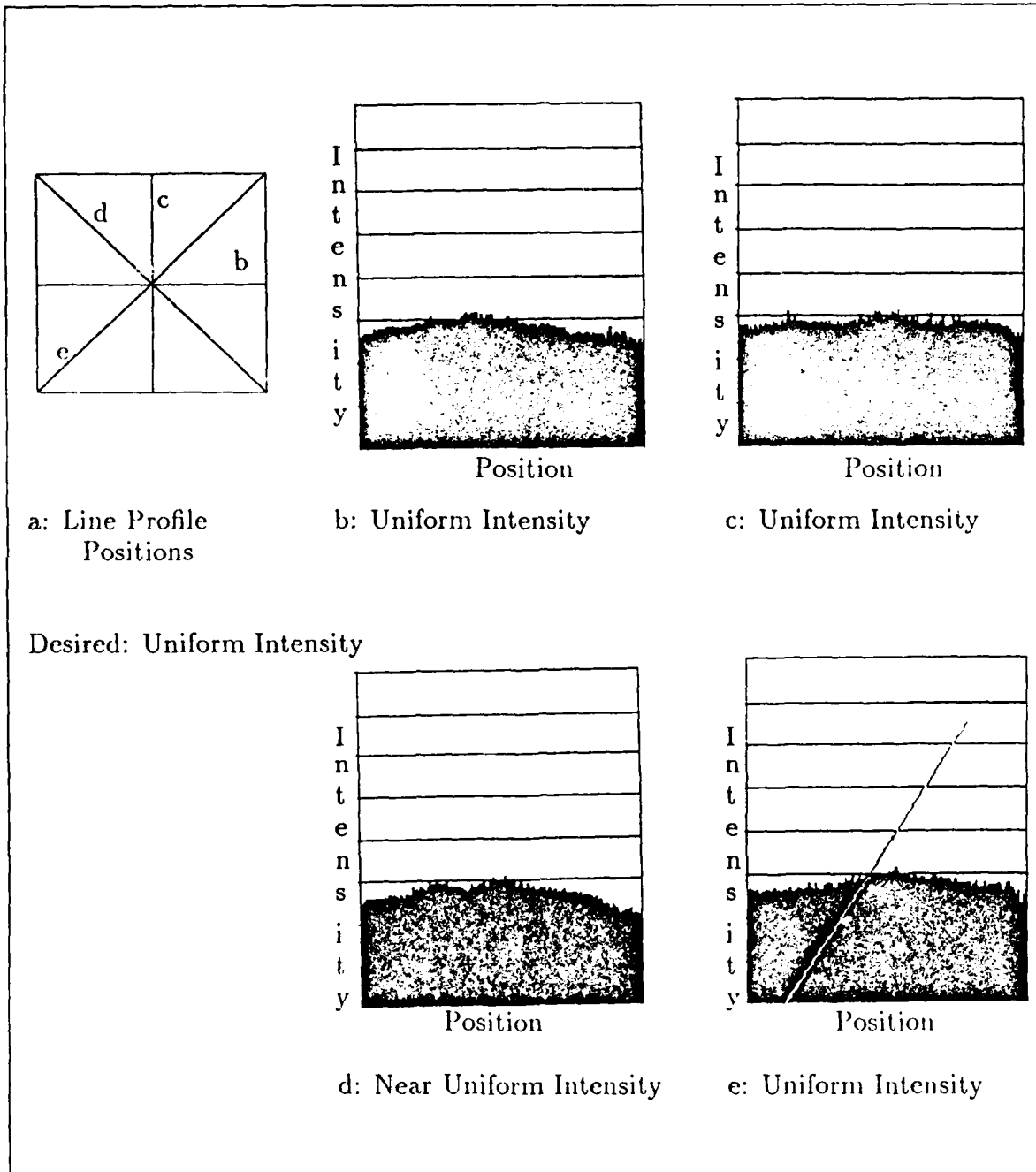


Figure 27. End Beam Wavefront Profiles

Appendix E. *Program for Calculating PSRI Moments*

The program used to calculate the PSRI moments is contained in this appendix. This program is written in BASIC. The values for "eta" were very small, which resulted in even smaller values for the PSRI moments. Multiplying all of the "eta" values by a constant does not effect the relations between the moments. Therefore, this program multiplies "eta" by 10^6 .

The program is given below.

```
10 REM Data must be placed at the beginning of the program.
20 REM This program has 18 vectors of data, each 10 numbers long.
240 DIM X(18)
250 DIM Y(18)
260 DIM FACT(4)
270 FACT(0) = 1
280 FACT(1) = 1
290 FACT(2) = 2
300 FACT(3) = 6
310 DIM ETA(18,3,3)
320 DIM PHI(18,7)
330 DIM MU(18,3,3)
340 DIM DIST(18,18)
350 DIM A(18,10)
360 I = 1
370 FOR I = 1 TO 18
380 J = 1
390 FOR J = 1 TO 10
400 READ A(I,J)
410 NEXT J
```

```

420 NEXT I
430 U$ = "####.##"
440 I = 1
450 FOR I = 1 TO 18
460 J = 1
465 FOR J = 1 TO 10
470 IF J = 1 THEN D(I,0,0) = A(I,J) ELSE
480 IF J = 2 THEN D(I,1,0) = A(I,J) ELSE
490 IF J = 3 THEN D(I,0,1) = A(I,J) ELSE
500 IF J = 4 THEN D(I,2,0) = A(I,J) ELSE
510 IF J = 5 THEN D(I,0,2) = A(I,J) ELSE
520 IF J = 6 THEN D(I,1,1) = A(I,J) ELSE
530 IF J = 7 THEN D(I,2,1) = A(I,J) ELSE
540 IF J = 8 THEN D(I,1,2) = A(I,J) ELSE
550 IF J = 9 THEN D(I,3,0) = A(I,J) ELSE
560 IF J = 10 THEN D(I,0,3) = A(I,J) ELSE GOTO 570
570 NEXT J
580 NEXT I
590 K = 1
600 FOR K = 1 TO 18
610 X(K) = D(K,1,0)/D(K,0,0)
620 Y(K) = D(K,0,1)/D(K,0,0)
630 NEXT K
640 V = 1
650 FOR V = 1 TO 18
660 N = 3
670 FOR P = 0 TO 3
680 Q = 0

```

```

690 FOR Q = 0 TO N
700 SUM = 0
710 R = 0
720 FOR R = 0 TO P
730 B = FACT(P)/(FACT(R) * FACT(P-R))
740 S = 0
750 FOR S = 0 TO Q
760 C = FACT(Q)/(FACT(S) * FACT(Q-S))
770 ADD = B * C * ((-X(V))^(P-R)) * ((-Y(V))^(Q-S)) * D(V,P,Q)
780 SUM = SUM + ADD
790 NEXT S
800 NEXT R
810 MU(V,P,Q) = SUM
830 NEXT Q
840 N = N - 1
850 NEXT P
880 NEXT V
890 L = 1
900 FOR L = 1 TO 18
910 N = 3
920 P = 0
930 FOR P = 0 TO 3
940 Q = 0
950 FOR Q = 0 TO N
960 ETA(L,P,Q) = (MU(L,P,Q)/(MU(L,0,0)^((2+P+Q)/2))) * 10^6
980 NEXT Q
990 N = N - 1
1000 NEXT P

```

```

1030 NEXT L
1040 C = 1
1050 FOR C = 1 TO 18
1060 PHI(C,1) = ETA(C,2,0) + ETA(C,0,2)
1070 PHI(C,2) = (ETA(C,2,0)-ETA(C,0,2))^ 2 + 4 * (ETA(C,1,1))^ 2
1080 PHI(C,3)=(ETA(C,3,0)-3*ETA(C,1,2))^ 2+ (3*ETA(C,2,1)-ETA(C,0,3))^ 2
1090 PHI(C,4)=(ETA(C,3,0)+ETA(C,1,2))^ 2 + (ETA(C,2,1) + ETA(C,0,3))^ 2
1093 CON=((ETA(C,3,0) + ETA(C,1,2))^ 2) - (3*(ETA(C,2,1)+ETA(C,0,3))^ 2)
1094 D = ETA(C,3,0) + ETA(C,1,2)
1095 B = ETA(C,2,1) - ETA(C,0,3)
1096 E = 3 * ETA(C,2,1) - ETA(C,0,3)
1097 A = ETA(C,3,0) - (3 * ETA(C,1,2))
1099 NUM = (3*(ETA(C,3,0)+ETA(C,1,2))^ 2 - ((ETA(C,2,1)+ETA(C,0,3))^ 2)
1100 PHI(C,5) = (A * D * CON) + (E * B * NUM)
1101 F = ETA(C,2,0) - ETA(C,0,2)
1103 H= ((ETA(C,3,0)+ETA(C,1,2))^ 2) - ((ETA(C,2,1)+ETA(C,0,3))^ 2)
1105 I=4 * ETA(C,1,1) * (ETA(C,3,0)+ETA(C,1,2)) * (ETA(C,2,1)+ETA(C,0,3))
1110 PHI(C,6) = (F * H) + I
1120 PHI(C,7) = (E * D * CON) - (A * B * NUM)
1130 NEXT C
1140 G = 1
1150 FOR G = 1 TO 18
1160 T = 1
1170 FOR T = 1 TO 7
1180 LPRINT PHI(G,T);
1190 LPRINT " ";
1191 NEXT T
1192 LPRINT

```

```
1193 LPRINT
1194 LPRINT
1220 NEXT G
1230 K = 1
1240 FOR K = 1 TO 18
1250 I = 1
1260 FOR I = 1 TO 18
1270 SUM = 0
1280 J = 1
1290 FOR J = 1 TO 7
1300 B = (ABS(PHI(K,J) - PHI(I,J)))^ 2
1310 SUM = SUM + B
1320 NEXT J
1330 DIST(K,I) = SUM^ (1/2)
1340 NEXT I
1350 S = 1
1360 FOR S = 1 TO 18
1370 LPRINT USING U$;DIST(K,S)
1371 LPRINT " ";
1390 NEXT S
1391 LPRINT " "
1400 LPRINT
1410 LPRINT
1420 LPRINT
1430 NEXT K
```


Bibliography

1. Athale, R. A. and others. "Use of E-Beam Written CGH in Pattern Recognition," Proceedings of the SPIE International Conference on Computer-Generated Holography, 437. 48-53. Bellingham, Washington: 1983.
2. Blodgett, J. A. and others. "Multiplexed Coherent Optical Processor for Calculating Generalized Moments," Optics Letters, 7: 7-9 (January 1982).
3. Casasent, David. "Scene Analysis Research: Optical Pattern Recognition and Artificial Intelligence," Proceedings of the SPIE in Optical and Hybrid Computing, 634. 439-456. Leesburg, Virginia: 1986.
4. Casasent, David and others. "Optical System to Compute Intensity Moments: Design," Applied Optics, 21: 3292-3298 (September 1982).
5. Casasent, David and R. Lee Cheatham. "Image Segmentation and Real-Image Tests for an Optical Moment-Based Feature Extractor," Optics Communications, 51: 227-230 (September 1984).
6. Casasent, David and Demetri Psaltis. "Hybrid Processor to Compute Invariant Moments for Pattern Recognition," Optics Letters, 5: 395-397 (September 1980).
7. ----- "Optical Pattern Recognition using Normalized Invariant Moments," Proceedings of the SPIE in Optical Pattern Recognition, 201. 107-114. Bellingham, Washington: 1979.
8. Freeman, Mark O. and Bahaa E. A. Saleh. "Moment Invariants in the Space and Frequency Domains," Journal of the Optical Society of America, 5: 1073-1084 (July 1988).
9. Gaskill, Jack D. Linear Systems, Fourier Transforms, and Optics. New York: John Wiley & Sons, 1978.
10. Goodman, Joseph W. Introduction to Fourier Optics. New York: McGraw-Hill Book Company, 1968.
11. Hu, Ming-Kuei. "Visual Pattern Recognition by Moment Invariants," IRE Transactions on Information Theory, IT-8. 179-187 (February 1962).
12. Kabrisky, Matthew E. Class lecture in EENG 620, Pattern Recognition I. School of Engineering, Air Force Institute of Technology (AU), Wright-Patterson AFB OH, January 1988.
13. Lee, Wai-Hon. "Computer-Generated Holograms: Techniques and Applications," Progress In Optics, Volume 16, edited by E. Wolf. New York: North-Holland Publishing Company, 1978.

14. Mayo, 2Lt Michael W. Computer- Generated Hologram and Magneto-Optic Spatial Light Modulator for Optical Pattern Recognition. MS thesis, AFIT/GEO/ENG/87D-1. School of Engineering, Air Force Institute of Technology (AU), Wright-Patterson AFB OH, December 1987.
15. Ruck, Capt Dennis W. Multisensor Target Detection and Classification. MS thesis, AFIT/GE/ENG/87D-56. School of Engineering, Air Force Institute of Technology (AU), Wright-Patterson AFB OH, December 1987.
16. Soroko, Lev Markovich. Holography and Coherent Optics, translated by Albin Tybulewicz. New York: Plenum Press, 1980.
17. Teague, Michael R. "Image Analysis via the General Theory of Moments," Journal of the Optical Society of America, 70: 920-930 (August 1980).
18. ----- "Optical Calculation of Irradiance Moments," Applied Optics, 19: 1353-1356 (April 1980).

Vita

Vicky L. Robinson was born on 4 August 1959 in Greeneville, Tennessee. She graduated from West Greene High School in Mosheim, Tennessee in June of 1977. She attended Tusculum College in Tusculum, Tennessee, graduating in May 1981. She received the degree of Bachelor of Science in Biology. She enlisted in the United States Air Force in February 1982 and received her commission in May 1982 upon graduating from Officers Training School. She then entered the Air Force Institute of Technology (AFIT) Undergraduate Engineering Conversion Program at the University of Southern Florida in Tampa, Florida and graduated Cum Laude in August 1984. She received the degree of Bachelor of Science in Electrical Engineering. Upon graduation, she was stationed at the Ballistic Missile Office at Norton AFB in San Bernardino, California. She entered the Electro-optics Masters Program in the School of Engineering, AFIT, in May 1987.

Permanent address: Route 1, Box 540
Midway, Tennessee 37809

14. Mayo, 2Lt Michael W. Computer- Generated Hologram and Magneto-Optic Spatial Light Modulator for Optical Pattern Recognition. MS thesis, AFIT/GEO/ENG/87D-1. School of Engineering, Air Force Institute of Technology (AU), Wright-Patterson AFB OH, December 1987.
15. Ruck, Capt Dennis W. Multisensor Target Detection and Classification. MS thesis, AFIT/GE/ENG/87D-56. School of Engineering, Air Force Institute of Technology (AU), Wright-Patterson AFB OH, December 1987.
16. Soroko, Lev Markovich. Holography and Coherent Optics, translated by Albin Tybulewicz. New York: Plenum Press, 1980.
17. Teague, Michael R. "Image Analysis via the General Theory of Moments," Journal of the Optical Society of America, 70: 920-930 (August 1980).
18. ----- "Optical Calculation of Irradiance Moments," Applied Optics, 19: 1353-1356 (April 1980).

Vita

Vicky L. Robinson [REDACTED]
[REDACTED]

She attended Tusculum College in Tusculum, Tennessee, graduating in May 1981. She received the degree of Bachelor of Science in Biology. She enlisted in the United States Air Force in February 1982 and received her commission in May 1982 upon graduating from Officers Training School. She then entered the Air Force Institute of Technology (AFIT) Undergraduate Engineering Conversion Program at the University of Southern Florida in Tampa, Florida and graduated Cum Laude in August 1984. She received the degree of Bachelor of Science in Electrical Engineering. Upon graduation, she was stationed at the Ballistic Missile Office at Norton AFB in San Bernardino, California. She entered the Electro-optics Masters Program in the School of Engineering, AFIT, in May 1987.

[REDACTED]
[REDACTED]

UNCLASSIFIED

SECURITY CLASSIFICATION OF THIS PAGE

REPORT DOCUMENTATION PAGE

Form Approved
OMB No. 0704-0188

1a. REPORT SECURITY CLASSIFICATION UNCLASSIFIED			1b. RESTRICTIVE MARKINGS		
2a. SECURITY CLASSIFICATION AUTHORITY			3. DISTRIBUTION / AVAILABILITY OF REPORT Approved for public release; distribution unlimited.		
2b. DECLASSIFICATION / DOWNGRADING SCHEDULE					
4. PERFORMING ORGANIZATION REPORT NUMBER(S) AFIT/GEO/ENG/88D-3			5. MONITORING ORGANIZATION REPORT NUMBER(S)		
6a. NAME OF PERFORMING ORGANIZATION School of Engineering		6b. OFFICE SYMBOL (If applicable) AFIT/ENP		7a. NAME OF MONITORING ORGANIZATION	
6c. ADDRESS (City, State, and ZIP Code) Air Force Institute of Technology (AU) WP AFB, OH 45433-6583			7b. ADDRESS (City, State, and ZIP Code) <i>Reviewed 10 Jan 1989</i>		
8a. NAME OF FUNDING / SPONSORING ORGANIZATION		8b. OFFICE SYMBOL (If applicable)		9. PROCUREMENT INSTRUMENT IDENTIFICATION NUMBER	
8c. ADDRESS (City, State, and ZIP Code)			10. SOURCE OF FUNDING NUMBERS		
			PROGRAM ELEMENT NO.	PROJECT NO.	TASK NO.
			WORK UNIT ACCESSION NO.		
11. TITLE (Include Security Classification) HYBRID CALCULATION OF INVARIANT MOMENTS (UNCLASSIFIED)					
12. PERSONAL AUTHOR(S) Vicky L. Robinson, Captain, USAF					
13a. TYPE OF REPORT MS thesis		13b. TIME COVERED FROM _____ TO _____		14. DATE OF REPORT (Year, Month, Day) 1988, December	
15. PAGE COUNT 64					
16. SUPPLEMENTARY NOTATION					
17. COSATI CODES			18. SUBJECT TERMS (Continue on reverse if necessary and identify by block number)		
FIELD	GROUP	SUB-GROUP	Pattern Recognition, Optical Processing		
12	09				
09	05				
19. ABSTRACT (Continue on reverse if necessary and identify by block number)					
<p>Thesis Advisor: Capt S. Rogers, PhD Associate Professor, Dept of Electrical and Computer Engineering</p> <p>A hybrid setup for computing a position, scale, rotation invariant (PSRI) feature set was investigated. The low order ordinary moments of a set of objects were first optically calculated. The detour phase hologram, a binary method, was used to produce wavefronts which were then imaged onto the image plane. The Fourier transform of the product of these two transmittances was taken and the resultant intensity pattern recorded. The center intensity value, or ordinary moment of the object, was then found using a frame grabber and Image-Pro software. The moment values were digitally processed to form a PSRI feature set. The ordinary and PSRI moments were tested for pattern</p>					
20. DISTRIBUTION / AVAILABILITY OF ABSTRACT <input checked="" type="checkbox"/> UNCLASSIFIED/UNLIMITED <input type="checkbox"/> SAME AS RPT. <input type="checkbox"/> DTIC USERS			21. ABSTRACT SECURITY CLASSIFICATION UNCLASSIFIED		
22a. NAME OF RESPONSIBLE INDIVIDUAL Steven K. Rogers, Associate Professor			22b. TELEPHONE (Include Area Code) (513) 255-6027		22c. OFFICE SYMBOL AFIT/ENG

19. recognition possibilities. The Euclidean distances between the objects were calculated, revealing the separation necessary for pattern recognition.